Compact design of a self-supported reflectarray-based subreflector for reflector antenna at 94 GHz

Jose Javier Rodríguez Días

School of Electrical Engineering

Thesis submitted for examination for the degree of Master of Science in Technology.

Madrid 23.11.2018

Supervisor

Univ. Lect. Jari Holopainen

Advisors

Univ. Lect. Miguel A. Salas

Prof. Jose A. Encinar Garcinuño

Aalto University
School of Electrical
Engineering

Aalto University
School of Electrical Engineering

Aalto University, P.O. BOX 11000, 00076 AALTO
www.aalto.fi
Abstract of the master's thesis

Author Jose Javier Rodríguez Días

Title Compact design of a self-supported reflectarray-based subreflector for reflector antenna at 94 GHz

Degree programme Master's Programme in Electronics and Nanotechnology

Major Radio Science and Engineering **Code of major** ELEC3038

Supervisor Univ. Lect. Jari Holopainen

Advisors Univ. Lect. Miguel A. Salas, Prof. Jose A. Encinar Garcinuño

Date 23.11.2018 **Number of pages** 55+1 **Language** English

Abstract

Due to the massive utilization of mobile communication channels, novel communication systems must work in higher frequency bands. These systems, such as microwave and satellite communications, require high gain antennas with a low profile due to their operational and deployment scenarios. Furthermore, the weight, calibration process, structural design and cost all lead to several manufacturing constraints. On the other hand, reflector antennas are less affected by these constraints. They are the best trade-off solution for these applications because of their simplicity and cost. In addition, the reflectarray antenna has similarly demonstrated its potential in the aerospace and automotive industry. For these reasons, this thesis examines the feasibility of synthesizing an axially displaced elliptical subreflector, part of a dual reflector antenna, thus continuing much needed research in new manufacturing techniques to decrease the profile of the reflector antenna as well as its cost. The analysis is performed using the W band, 94 GHz, which is used for small space object detection at long range. The outcomes are obtained through computational software, such as GRASP for physical optics analysis, CST for electromagnetic simulations, MATLAB for high-density calculations, and MRADANT-UPM for the reflectarray synthesis in microstrip technology. The results reveal that this technology is still in its infancy; thus, new avenues are suggested for further research. For example, the methodology used needs more development in areas, such as computational analysis efficiency.

Keywords Satellite antenna , splashplate , reflector antenna , hat-fed , subreflectarray , W band , axially displacement , reflectarray , self-supported feed , phase shift

Preface

First of all, I would like to thank Aalto University for accepting me to the Master of Science programme, as well as to the Students Union (AYY) for the essential work they do for us students. Thanks must also be extended to Opetus- ja kulttuuriministeriö (OKM) and to the citizens of Finland who support education in some many ways. Special gratitude to the professors, teachers and assistants who allowed me to participate in the world of academia inspiring and motivating my desire to learn. Those game changers: Ari Sihvola, Keijo Nikoskinen, Jari Holopainen, Clemens Icheln, Ville Viikari, Anya Siddiqi, Sami Suihkonen, Henrik Wallén, Jaan Praks, Jussi Ryynänen, Luis de Jussilainen Costa, Dimitrios C. Tzarouchis , Jari-Matti Hannula, Katsuyuki Haneda, Annika Salama, Juha Ala-Laurinaho, Juha Mallat, Antti Räisänen, Esa Kallio, Konstantin Simovski, Jari Hänninen, Anu Lehtovuori, Teppo Huhtio, Markku Sopanen, Ilkka Tittonen, and many others in the Department of Electronics and Nanoengineering of Aalto University. I would also like to express my gratitude to the International Office, especially to Helena Hietanen and Niina Huovinen for supporting me during my exchange experience.

In addition, I would like to commemorate Mariano Barba Gea for his inspiration and guidance during my exchange period in Madrid. Wherever you are, already in June 2014, your outstanding work and inspiring teaching awakened in me a passion for working in the lab. Many thanks to Jose Antonio Encinar, for his lessons, patience and experience, particularly at the end of the thesis. Miguel Salas was also of great help in giving me the opportunity to work in the antenna industry, while I simultaneously wrote this thesis.

The work was developed in UPM, Madrid from June 2017 to December 2018 under challenging circumstances. At first, the topic was related to the study of displaced axis parabolic reflectors. Unfortunately, my first thesis advisor, Mariano Barba, passed away during the initial phase of my thesis work, thus causing a change in topic. In the period between the topic changes, summer 2017, I developed a hat-fed system called BarbaHat, in honour of Mariano Barba Gea.

Finally, this thesis is dedicated to my loved ones, to my parents, Lucía and Jose, to my siblings, Roberto and Ana, as well as to my life partner, Sara. And last, but not least, to my friends, especially the new ones made in Finland. It has been an amazing trip.

Madrid, 23.11.2018

Jose Javier Rodríguez Días Engineer

Contents

Abbreviations

AD	axially displaced
ADE	axially displaced elliptical
CWG	circular waveguide
DOMSS	design and optimization Matlab set of scripts
EM	electromagnetic
FDTD	finite difference time domain
FM	full metal
FR	flat-ring
GUI	graphical user interface
HPBW	half-power beamwidth
LNA	low noise amplifier
MoM	method of moments in spectral domain
MRADANT-UPM	multilayer reflect-array: design and analysis antenna tool from UPM
PEC	perfect electric conductor
PO	physical optics
RA	reflectarray
REF	reference
SLL	side-lobe level
SOTM	satellite on the move
SWR	standing wave ratio
VSWR	voltage standing wave ratio
XP	cross polarization

1 Introduction

Over the last decade, long distance communications systems have required an increased transmission rate due to saturation of the spectrum as well as the increase of users which has forced these systems to work in higher frequency bands [1]. In the scenario of satellite communications where distances are larger, these systems require high gain antennas. Traditionally, configuration of the phase array antenna has been the most used option due to its versatility; however, as there is a need for a complex feeding network for the elements of the array, this configuration renders this solution less attractive and more costly [2]. Additionally, systems, such as SOTM (satellite on the move), require cost-effective antennas which are low profile and light in weight, as well as in the case of space missions. Alternatively, reflector antennas are highly directive and composed of less components. Since the directivity is proportional to the aperture size of the reflector, the required high gain is facilitated with a reflector antenna. This alternative configuration is used in many applications, such as mobile backbone, point-to-point links, remote sensing, satellite tracking, radar systems, radio astronomy, satellite communications, and deep space communications. In the case of small terminals or stations, these antennas are widely used because of their relatively low cost, easy maintenance and light weight. Reflector antennas are manufactured with different materials, such as carbon fibre for a man-pack or satellite on the move (SOTM) applications. For example, metal reflector grids are used for small terminals and fixed stations, whereas solid reflector sheets are applied to large and high accuracy systems, such as radio telescope for deep space exploration [1]. For on-board space applications, ultra-thin reflectors are manufactured with composite materials. These are assembled into a sandwich configuration based on a honey-comb structure supporting thin layers of aluminium or carbon [3]. This manufacturing technology is highly suited to creating shaped reflector antennas, especially in space applications where customized coverage is needed, such as in broadcasting satellite systems.

Due to the need for a higher frequency band, such as the W band, this work is centred on the frequency of 94 GHz [4, 5, 6]. At this band, undesired effects occur reducing the efficiency and challenging the features of the antenna. Furthermore, manufacturing techniques are under research and development.

The objective of this thesis is to determine the feasibility of implementing a novel technique to a self-supported feed system that reduces the weight, the cost and profile, while simultaneously preserving the features of the antenna. This is accomplished by synthesising the subreflector in a planar substrate, such as in microstrip technology. Attached to a horn antenna, this subreflector is part of a self-supported feed. It reflects the energy backwards in the direction of the main reflector. This method aims to reduce the profile by increasing the feed subtended angle ϕ_M and the focal length to diameter (f/D) ratio of the main reflector.

The phase delay introduced by the reference subreflector is calculated with the form of a matrix. Each value of this matrix is reproduced by a phase shifter element or cells. Thus, by printing patch cells on the substrate with different characteristics, the same phase shift is produced by the planar surface with similar behaviour to the reference curved surface.

This thesis starts with the theoretical framework in chapter 2, where the required basics are explained. It begins with a brief section of antenna definitions, it follows with reflector geometry notions and reflectarray concepts to end with the state-of-the-art, where research material is presented regarding new geometries and self-supported feeds. Chapter 3 continues with the work contribution, the design methodology and results. The conclusion of the synthesis methodology is presented in chapter 4.

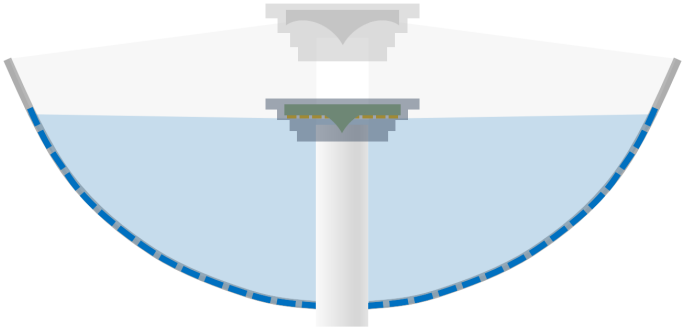

Figure 1: Example of the subreflector synthesis.

2 Fundamentals of antennas and reflectarray

The first section of this chapter describes fundamental aperture antenna concepts. It provides a decomposition of the directivity as a function of the efficiency factor. This factor is divided in sub-efficiencies which are referenced throughout the document illustrating aperture antenna development. Secondly, classical reflector geometries are presented: single and dual configurations. The evolution of these from prime vertex, or classical reflectors, to ring vertex reflectors, is described by presenting axially displaced (AD) reflector geometry. These configurations increase the efficiency of the antenna when applied to the main reflector. However, it requires a ring focus feed to illuminate the reflector. Therefore, axial displacement is also explained as applied to an elliptical subreflector. Thus, the final configuration of the antenna is a self-supported ring focus feed with a ring vertex reflector. The objective is to synthesize the subreflector with reflectarray technology. Thus, this chapter presents the fundamental concepts and geometry details to end with the latest research conducted in the field.

2.1 Definition and fundamental concepts

Directivity $D(\theta, \phi)$ is the most significant parameter of an antenna [7]. It is defined as the power density ($\wp(\theta, \phi)$) radiated in a certain direction to a certain distance, with respect to the same power density radiated by an isotropic antenna which would have radiated the same power.

$$D(\theta, \phi) = \frac{\wp(\theta, \phi)}{P_{radiated}/4\pi r^2} \tag{2.1}$$

If the angular direction is not specified, it is assumed the directivity at the maximum radiation direction,

$$D = \frac{\wp_{max}\ 4\pi r^2}{P_{radiated}} \tag{2.2}$$

Defining the normalized radiation pattern as,

$$t(\theta, \phi) = \frac{\wp(\theta, \phi)}{\wp_{max}} \tag{2.3}$$

Maximum directivity can be also obtained through the normalized radiation pattern where Ω_e is the equivalent solid angle,

$$D = \frac{4\pi}{\iint_{4\pi} t(\theta, \phi)\, d\Omega} = \frac{4\pi}{\Omega_e} \tag{2.4}$$

In antennas with a main lobe and some reduced secondary lobes, such as reflector antennas, the directivity can be estimated. Assuming an uniform radiation in the solid angle, which is defined by the width of the beam at -3 dB on main radiation planes ($\Delta\theta_1 \cdot \Delta\theta_2$), the Directivity results as,

$$D = \frac{4\pi}{\Omega_e} = \frac{4\pi}{\Delta\theta_1 \cdot \Delta\theta_2} \tag{2.5}$$

When known maximum directivity D and normalized radiation pattern $t(\theta, \phi)$, the directivity in any direction can be obtained directly by the product of both,

$$D(\theta, \phi) = D\ t(\theta, \phi) \tag{2.6}$$

A second parameter directly related with directivity is the gain ($G(\theta, \phi)$). Its definition is similar, but the ratio is not given with radiated power, but with power delivered to the antenna. This allows to take into account the losses introduced by the antenna, which are not delivered to the space. Consequently, directivity and gain are related by the **efficiency**, η_t, of the antenna,

$$G(\theta, \phi) = \frac{\wp(\theta, \phi)}{\frac{P_{delivered}}{4\pi r^2}} = \frac{P_{radiated}}{P_{delivered}} \frac{\wp(\theta, \phi)}{\frac{P_{radiated}}{4\pi r^2}} = \eta_t D(\theta, \phi) \tag{2.7}$$

Ideally, the lossless antenna has equivalent directivity and gain,

$$D(\theta, \phi) \equiv G(\theta, \phi) \tag{2.8}$$

In the case of **single** reflector antennas, two radiation patterns are considered. The primary one belongs to the feed, and the secondary one to the reflector when it is illuminated by the feed (Fig. 2). Generally, there is a certain amount of power which is not intercepted by the reflector when it is illuminated. The feed radiates P_r but only part of this power, P_a, is intercepted by the surface of the reflector, therefore $P_r - P_a$ is not contributing to the secondary radiation pattern.

$$D = \frac{\wp_{max}\ 4\pi r^2}{P_a} \frac{P_a}{P_r} \tag{2.9}$$

This over-illumination is called spillover and it is represented by the spillover efficiency,η_s. Normally it is interesting the lowest as is possible [7].

$$\eta_s = \frac{P_a}{P_r} \tag{2.10}$$

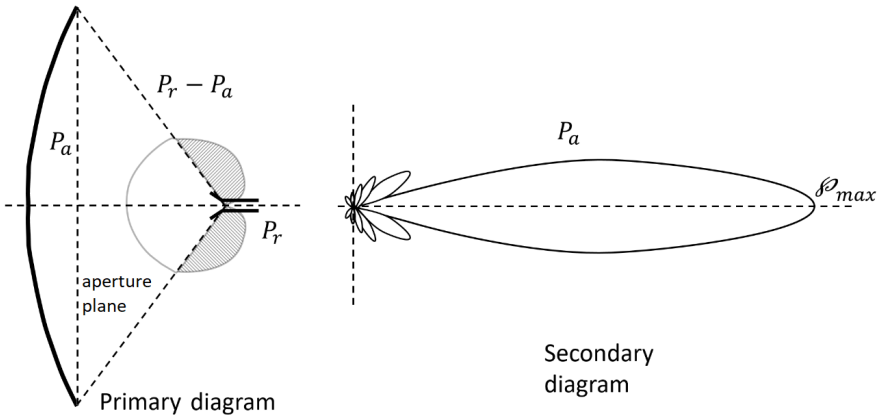

Figure 2: Power balance of a parabolic reflector [7].

The power P_a at the rim of the reflector presents a field distribution with the form of

$$\vec{E}_a(\rho', \phi') = E^a_{cp}(\rho', \phi')\hat{e}_{cp} + E^a_{xp}(\rho', \phi')\hat{e}_{xp} \tag{2.11}$$

where E^a_{cp} and E^a_{xp} are respectively the reference and the cross polarized field distributions produced at the aperture plane. The radiated power associated to each polarization are, the co-polar P_{cp} and the cross-polar P_{xp}. In the case where there is a polarization of reference, there is also the implicit efficiency η_x, defined as the ratio of the reference polarization power to the total radiated power.

$$\eta_x = \frac{P_{cp}}{P_a} \tag{2.12}$$

Therefore, the equation (2.2) can be written as,

$$D = \frac{\wp_{max}\ 4\pi r^2}{P_{cp}} \frac{P_{cp}}{P_a} \frac{P_a}{P_r} \tag{2.13}$$

As stated, the rim of the reflector is modelled as an aperture antenna, with a finite geometrical area that radiates the distributed field $\vec{E}_a(\rho', \phi')$. This area produces a non uniform illumination. Assuming the Huygens' principle, the energy is attenuated by the natural spherical spreading of a punctual source of radiation. In addition, this source of radiation discriminates the energy in the space with the form of the radiation pattern [7]. The effect of these two factors called edge taper is explained in the context of chapter 2.2.1. The directivity of the total antenna is affected by the mentioned losses. The equation of the aperture antenna directivity expressed as a function of the illumination efficiency η_{ill}, is compared with the equation (2.2).

$$D_{aperture} = \frac{4\pi}{\lambda^2}\ A_{geometric}\ \eta_{ill} = \frac{\wp_{max}\ 4\pi r^2}{P_{cp}} \tag{2.14}$$

The directivity of the aperture antenna system including the efficiencies previously defined is given below.

$$D = \frac{\wp_{max}\ 4\pi r^2}{P_{cp}} \frac{P_{cp}}{P_a} \frac{P_a}{P_r} = \frac{4\pi}{\lambda^2}\ A_{geometric}\ \eta_{ill}\eta_x\eta_s = \frac{4\pi}{\lambda^2}\ A_{geometric}\eta_t = \frac{4\pi}{\lambda^2}\ A_{eff} \quad (2.15)$$

Thus, the total efficiency, η_t, is obtained by the product of spillover, η_s, polarization,η_x and illumination efficiency, η_{ill}. These factors and its impact are commented along the text.

$$\eta_t = \eta_s\eta_x\eta_{ill} \quad (2.16)$$

There are some other efficiencies derived from design aspects, such as reflector roughness, blockage, input-mismatch that are present depending on the reflector configuration [3].

2.2 Reflector antenna configuration

Reflector antennas have been used since the beginning of the radio era on the late of XIX century. However, it was at the end of Second World War when these antennas have suffered a huge investigation [7]. Reflector antenna results of locating a metallic sheet in front of a radiating source. The fields emanating the source, collide into the sheet and induce currents on the metallic surface. These currents, reproduce induced fields which are radiated outwards the structure [1]. The metallic sheet might be planar, for instance, the diedric reflector of the Yagi-Uda antenna[2]. Although, highly directive antennas are often parabolic. The paraboloid provide a focused beam on the desired direction with interesting features, such as small beam-width and low side-lobe level (SLL)[7]. The beam-width is usually measured at -3 dB from the maximum gain and it is called half-power beamwith (HPBW).The SLL is the ratio of power density in the adjacent lobe with respect to the main lobe.

2.2.1 Single or classical configuration

Classical configuration consist of a single reflector illuminated from a punctual source. Most of the reflectors are based on conic curves. Usually the source is a feed horn antenna. For instance, the phase centre of a feed horn antenna, which is a point, is located at the focus of the parabolic main reflector.

The feed horn is modelled as a Huygens source producing a spherical phase front. The phase centre of the horn is defined as the point where the front phase becomes identified as spherical [8, 9]. The spherical front is transformed into a plane wave front due to the mathematical properties of the parabola. The rays colliding the paraboloid, by Snell's law, are directed towards the directrix line located in the infinite [7]. The plane wave front reflected of the reflector is characterized with constant amplitude and planar phase front. By physical optics (PO), parallel rays provided by the paraboloid, creates a collimated beam which focuses on the infinite and produces minimum energy spreading [7, 10].

If specific radiation pattern is desired, the reflector is shaped accordingly. The shape of the reflector define the characteristics of the surface currents distribution [3]. The distribution at the aperture plane determines the beam. In fact, radiation pattern is computed applying 3D Fourier transformation to the current aperture distribution. Therefore, radiation pattern is directly related with the phase front produce by the shape of the reflector. The phenomena is illustrated in Figure 3. The phase front provided by the shaped reflector (b) is not planar compared with the non shaped (a).

[1] Induced currents method, physical optics and aperture method.
[2] Diedric case is normally analysed by the image theorem.

The analytical equation of the parabolic surface (Eq. (2.17) is transformed from cylindrical to polar coordinates in order to analyse the feed illumination angle ψ_0 .

$$r^2 = 4f(f+z) \rightarrow \rho = \frac{f}{\cos^2(\psi/2)} \tag{2.17}$$

where F is the focal length, ψ the half-subtended angle from the negative z-axis (Fig. 5). The reflector diameter is D and ρ is the family of rays from $\psi = 0$ to ψ_0, the value of the half subtended angle. The subtended angle is the illumination angle from the axis to the edge of the reflector. The aperture plane is located at the rim of the reflector at z_0 [9],

$$z_0 = D^2/16f \tag{2.18}$$

By defining the focal length f, it is also defined the focal length to diameter f/D ratio, which allows to remove the dimensions on the reflector analysis. The half subtended angle ψ_0 establishes the illumination angle from the feed [9],

$$\psi_0 = 2tan^{-1}\frac{D}{4f} \tag{2.19}$$

Figure 4 provides a scale [9] which relates the half subtended angle and the f/D parameters.

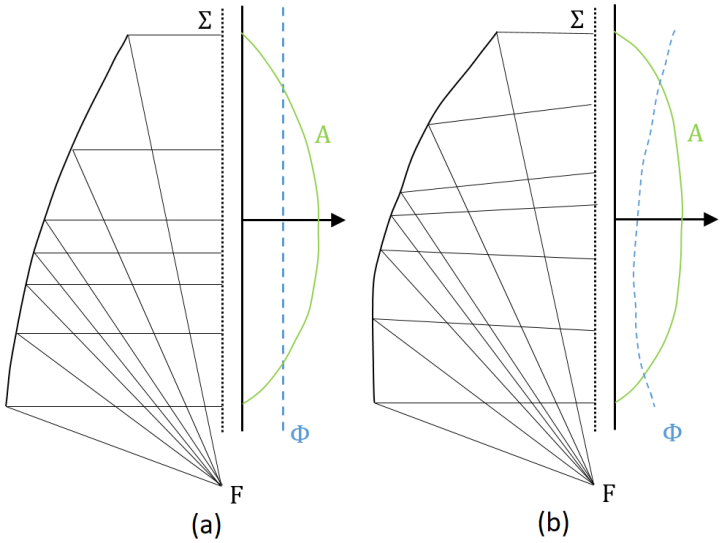

Figure 3: Parabolic offset reflector (a) and shaped reflector (b) phase and amplitude distributions [3].

At the half subtended angle ψ_0, the amplitude of the illumination defines the edge taper parameter which is, in other words, the illumination level at the edge of the reflector. This is an important factor that impacts the aperture efficiency through

the spillover efficiency (η_s) [11]. The feed horn antenna radiates the energy spatially discriminated as a function of the directivity pattern $t(\theta, \phi)$. Additionally, the wave front from the phase centre is attenuated as spherical source. Therefore, the illumination level on the edge of the reflector depends on those two factors, the directivity at the edge angle $t(\phi, \psi_0)$, and the added edge taper related with the spherical wave spreading from the focal point [7]. The edge taper is calculated by means of the equation (2.20, which comes from the superposition of the power density at a given angle, $\psi = \psi_0$, with respect to the power density on the axis of the parabola, $\psi = 0$ [7]. It is chosen such that the edge taper at the aperture plane is $\approx$ -12 dB. This value results from the diffraction and blockage losses trade-off related with the scale on Fig. 4 and detailed on [9]. Reflectors with high f/D, which are shallower, have larger edge taper than reflectors with lower f/D ratio.

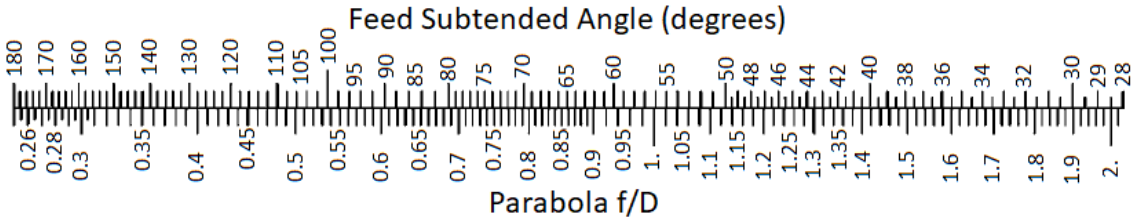

Figure 4: Scale for f/D and ψ_0 parameters relation [9].

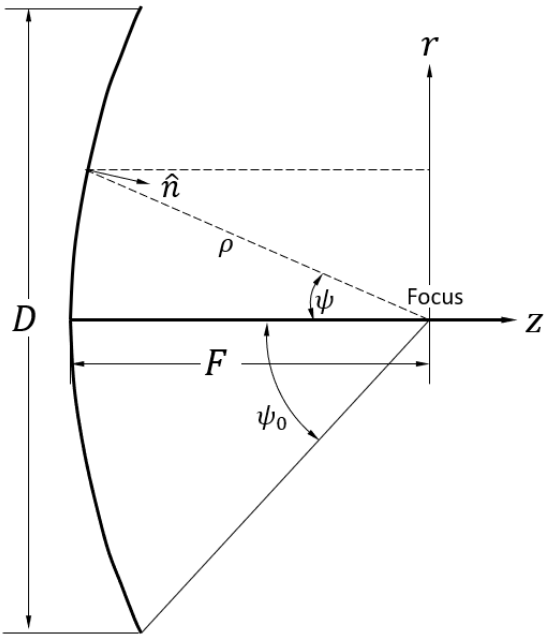

Figure 5: Parabolic reflector geometry in cylindrical and polar coordinates [9].

For instance, if the feed illuminates with -10 dB, respect to the maximum directivity, at the reflector edge angle $\psi_0 = 53.13°$, the added edge taper value resulting from the first part of Equation (2.20) which belongs to the spherical wave spread, is -1.94dB. Therefore, the aperture edge taper is -11.94 dB.

$$edge\ taper = 20\ \log(\cos^2(\psi_0/2)) + 10\ \log(t_f(\theta,\phi))\ (dB) \tag{2.20}$$

These notions apply to single reflector configuration (Fig. 5). Single configuration requires struts in order to support the feed at the focal point, as well as transmission lines from the feed to the transmitter (or receiver). Struts have a significant effective area and they behave as dipoles [7]. This impacts the radiation pattern reducing directivity and increasing side-lobes and cross polarization level which is translated in a detriment of efficiency [8]. These are partially solved by implementing the offset-fed configuration (Fig. 6) which is illuminated from out of the aperture line of sight. This setup allows convenient packaging for fitting into small space, for instance a spacecraft. However, this solution produces high cross-polarization level in y-axis (in the coordinate system of the figure) for shallow (high f/D) reflectors [7].

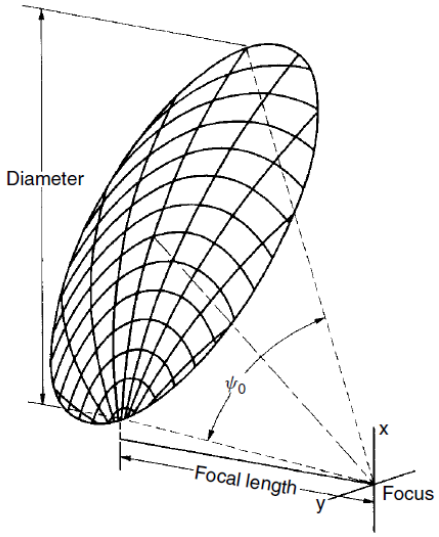

Figure 6: Offset-fed paraboloidal reflector [9].

Furthermore, due to the location of the feed and the low noise amplifier (LNA), single reflector configuration implies the need of long enough guided transmission lines, which introduces losses affecting the efficiency of the entire antenna system. Other disadvantages of front-fed parabolic reflectors are cooling or waterproofing the feed due to the same reason [9, 11].

2.2.2 Dual reflector configuration

As a solution to the mentioned drawbacks, dual reflector configuration is developed. Dual reflector derive from the optic telescope configuration, also known as dual mirror telescope [7]. The geometry consist on the insertion of a second reflector also with the shape of a conic curve and defined as subreflector (Fig. 7). Assuming as valid all the principles previously explained, it must be considered the focus coincidence between two different conic curves. In other words, the path of the rays travelling from the feed to the main reflector focus is extended. In the same way as a mirror in front of another mirror, the rays converge in the focus point, and that point can be considered as a new source of rays travelling to another conic curve. This way, the energy is transferred from one curve to another being perfectly focused.

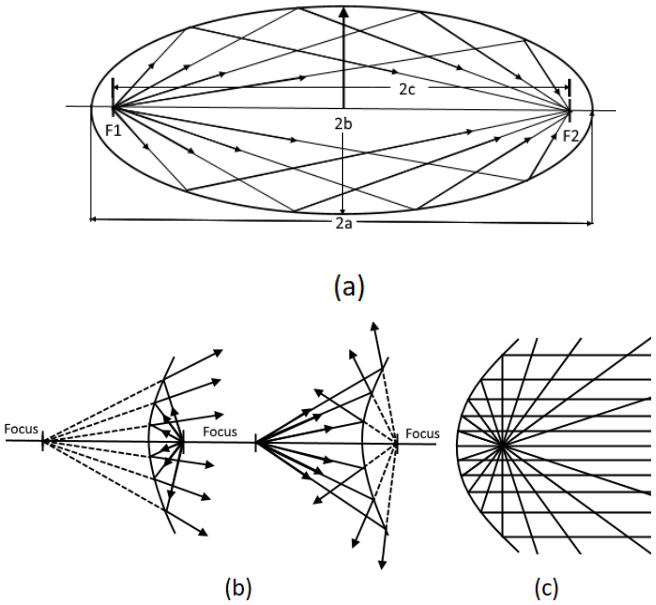

Figure 7: Conic curves ray tracing of Ellipse (a), Hyperbola (b) and Parabola (c).

Cassegrain configuration implements a hyperbolic subreflector and Gregorian uses an elliptical one (Fig. 8). For instance, in the Gregorian case (Fig. 7,8) the phase centre of the feed horn antenna is located at the focus *F1* of the ellipse, and the focus *F2* is coincident with the focus of the parabola, which is located closer of *F1*. Dotted rays converge to a virtual focus [9]. Cassegrain case is performed similarly. Thus, the feed illuminates the subreflector and the energy is reflected illuminating the main reflector. Dual reflector configuration allows the refrigeration of the transmitter (receiver) because the feed is located close to the vertex of the reflector, reducing the length of the transmission lines, as well as noise and losses [7, 9, 11].

As is mentioned, conic curves produce a focused beam. In fact, rays converge either

to a real or virtual focal point or to the directrix line in the parabolic case. Each conic curve owns two foci, and the rays travel from one focus towards the other. For this reason, conic curves applied to surfaces are commonly used for reflector antennas. In the case of the ellipse, both foci are real. If one of these is pushed through the infinite, the curve results into a parabola. Alternatively, if it is pushed to the negative axis, it results into a hyperbola [7].
Ray path is constant because of the mathematical properties, hence it is the perfect geometry to redirect a family of rays with no phase variation [12]. The ellipse and the hyperbola keep the spherical wave fronts, but they redirect the rays to a different focal point.
As is stated, Cassegrain configuration uses a hyperboloid as subreflector, while Gregorian uses an ellipsoid. However, there are much more Cassegrain systems implemented because Gregorian requires larger subreflector support. This is because the distance between the vertex of both reflectors is larger [9]. In short, struts supporting the subreflector are required in classical dual reflector configurations. Therefore, the effective area is reduced by subreflector and struts blockage, $\eta_{blockage}$ reducing efficiency [7, 9].

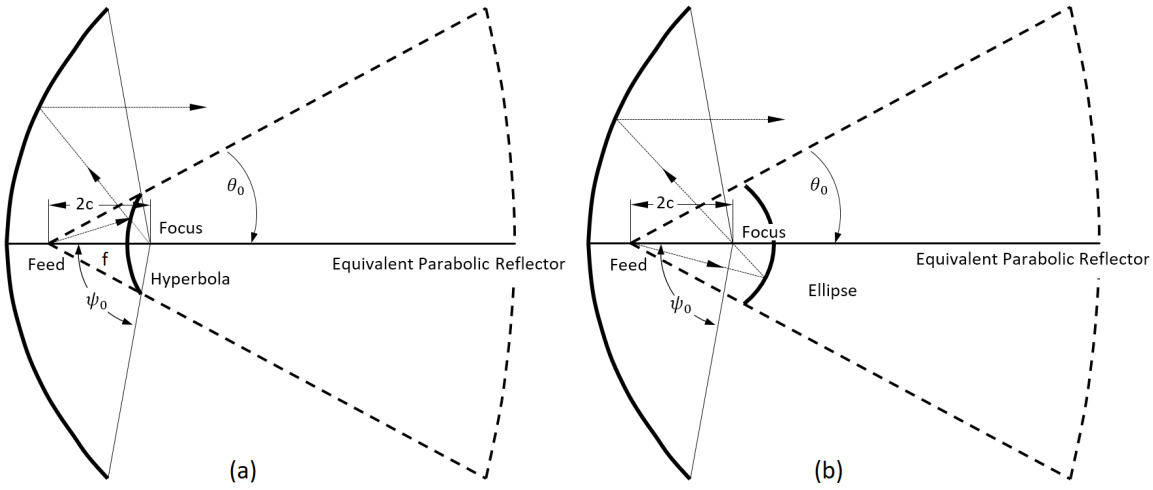

Figure 8: Cassegrain (a) and Gregorian (b) dual reflector configuration [9].

2.2.3 Axially Displaced reflector configuration

Up to this point, it is explained how to produce highly directive dual reflector antennas. Their advantages and drawbacks, for instance, it is possible to manage higher transmission power due to transmitter cooling. In addition, it helps in noise reduction in the LNA compared with single configuration. However, the blockage of the aperture is an issue. Displacing the axis of the conic curve before the axial revolution, produces a main reflector surface with a hole in the middle (Fig. 9), the ring vertex. The focus of the on-axis paraboloid is transformed in a ring focus. This is an AD reflector. It improves the efficiency of the reflector because it makes the most of the parabolic aperture with absence of shadows. This geometry is developed because of the need to make the most of the reflector aperture. By means of displacing the axis, the area previously blocked by the subreflector, is now transformed into a non-excitation area (Fig. 9) [9]. The subreflector is also axially displaced in order to create a ring focus subreflector, which matches with the ring vertex paraboloid. This allows the rays illuminating the main reflector never come back to the subreflector (Fig. 9). Consequently, by this configuration higher aperture efficiency (A_{eff}) is achieved.

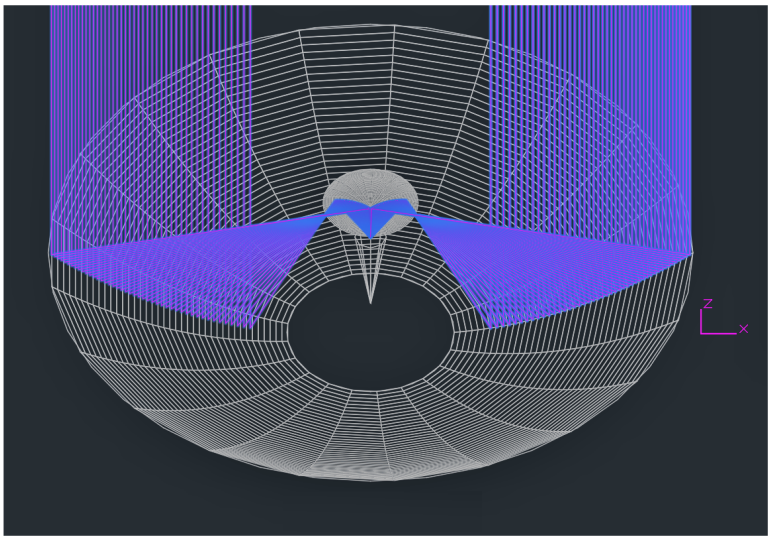

Figure 9: Axially displaced dual reflector.

The axially displaced elliptical (ADE) reflector implemented in this thesis is based on the Gregorian configuration (Fig. 8). The axial displacement procedure is given below (Fig. 10). The reflective properties of the parabola and the ellipse are assumed [9]. From Figure 8 (b), the lower half portion of the parabola and the upper portion of the ellipse are kept, the rest is removed. The result is shown in Figure 10, the green portion of the ellipse and the black .

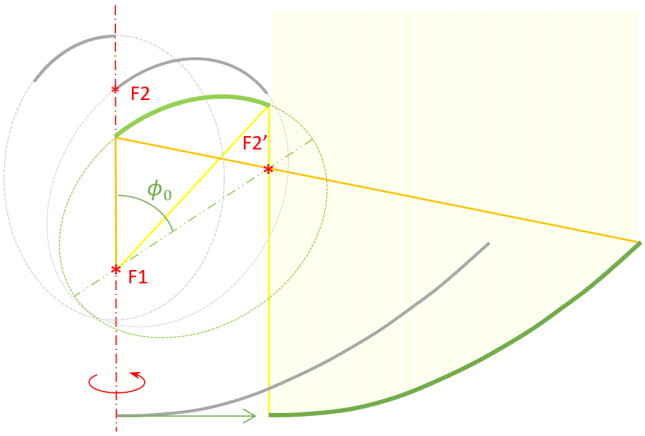

Figure 10: Elliptical reflector tilting procedure.

In the Figure 10, solid grey line is the initial subreflector which corresponds with Gregorian design. The portion of the parabola is displaced being the green colored the result (Fig. 11). The ellipse is tilted such that the focus *F1* is the tinting axis. The tilt angle, ϕ_0 has to be such that the focus *F2'* coincides with the focus of the parabola. Note that the horizontal limits of this axially displaced elliptical reflector are established by *F1* and *F2'*, as well as the initial point for the main reflector since its axis has been displaced from the projection of *F1* to the projection of *F2'*. This is because the furthest ray reflected in the subreflector (yellow) is the closest ray incident in the main reflector and vice versa (orange). Dual reflector geometry in two dimensions occurs when a specular reflection is applied (Fig. 11). Next, it is revolutionized symmetrically obtaining the axially displaced dual reflector in three dimensions.

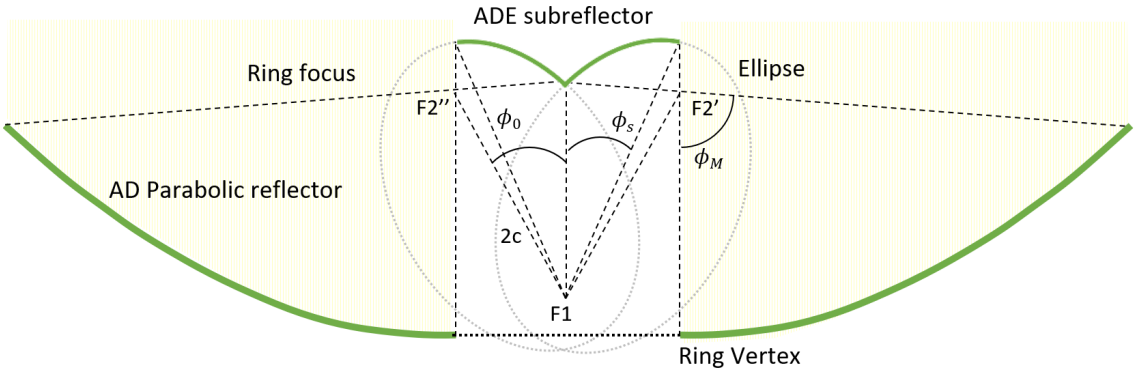

Figure 11: Axially displaced parabolic reflector antenna with axially displaced elliptical subreflector [9].

Furthermore, the subreflector is attached to the feed horn antenna by means of a dielectric or a radome. Hence, there is no need of struts because both, the feed horn antenna and the subreflector, are supported by the circular wave guide that behaves as a mast. This concept is called self-supporting subreflector. As stated, when the ellipse is tilted, the ring focus is produced. At the end of the process, the focus *F2* is splitted in *F2'* and *F2"*, both are part of the final ring focus of the AD reflector system. The same occurs to the vertex of the paraboloid, it becomes a ring vertex. Thus, the subreflector matches a ring focus with ring vertex of the main reflector. The radius of the subreflector is fixed by the distance between *F2'* and *F2"*. The radiating source is located at the focus *F1*[9]. Because the feed horn antenna illuminates the ADE subreflector with a Gaussian beam, higher density of energy is distributed at the centre of it. This type of subreflector inverts the rays, hence the main reflector illumination is inversely distributed. This effect causes higher allocation of rays at the outer rim of the AD parabolic main reflector [9]. In this sense, the highest amount of energy radiated or sensed, is located at the more effective areas of the main reflector, where there is not screws, blocking areas or diffractors.

2.3 Reflectarrays

Reflectarray, as its name indicates, combines reflector and phased array antenna advantages. These are, the simplicity when feeding the antenna which comes from the reflector and implies low losses in comparison with phased arrays, as well as the possible implementation over planar substrates. Furthermore, it is also inherited from the phased array antenna, the beam steering, multi-beam, contour beam and steerable or reconfigurable beam capabilities. Reflectarray is suitable for high directive and focused beam, dual polarization, as well as it supports dual frequency band. However, the major limitation of reflectarray system is related to the narrow bandwidth produced by the elements, although it has recently overcome, for instance, by stacking the elements [13].

The antenna concept was introduced on 1963 with waveguide elements. However, the interest on low-profile printed antennas on 1980 raises the research about reflectarray. Traditionally, parabolic reflectors have been used when highly directive antennas are needed. Therefore, reflectarray is the compromise solution which attempts to solve the disadvantages of both, parabolic reflector and conventional array. The goal is to implement the reflectarray technology on the subreflector for making the axially displaced dual reflector more compact [13].

Reflectarray can be either flat or slightly curved. The antenna is composed by radiating elements grouped in array configuration which are illuminated by a Gaussian beam produced by a horn antenna. The radiating elements can be open-ended waveguides, printed microstrip patches, dipoles or rings without any other passive components such as power dividers. As is stated, there are several methods of reflectarray elements implementation which produce a planar phase front. The phase control at each element is done depending on the element implementation method. One is to use microstrip patches (Fig. 12) with identical size and a phase delay transmission line attached to them.

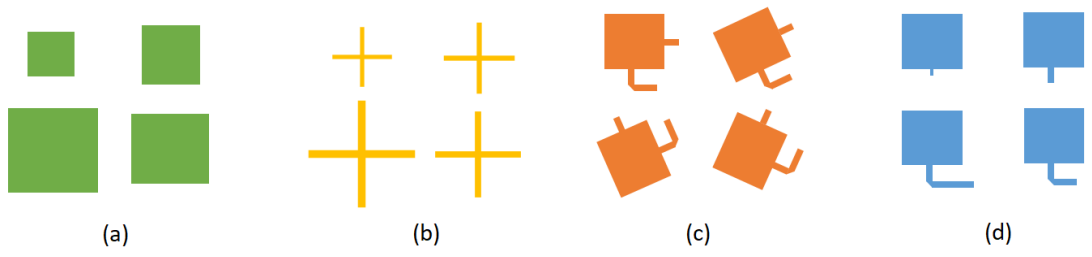

Figure 12: Reflectarray elements [13]. Resonant patches with different sizes (a), dipoles (b), patches sequentially rotated (c) and patches with stubs connected (d).

The transmission line attached to it is a stub, which compensates the phase shift

introduced by the different paths from the radiating source, the feed horn antenna. This element introduces losses and spurious radiation due to the stubs. Other option is to rotate the element sequentially or to use size-variable patches, rings or dipoles. Alternatively, other phase concepts have been investigated, such as aperture-coupled patches with stubs that allows to introduce active elements or controllable phase shifters; Vivaldi elements, Fresnel reflectors, apertures with variable size, concentric rings and multi-resonant elements [13].

Reflectarray elements are sensitive to the direction of the incident field, thus it is able to behave as a polariser. In addition, they are sensitive to the frequency of the incident field, hence, they are able to behave as a filter. Moreover, the elements are also sensitive to the incidence angle of the field, which corresponds with the behaviour of a lens. The operation principle assumes all the elements of the array in the far field. It is also assumed, that each element of the array is illuminated with an oblique incident field. Assuming the Floquet conditions corresponding with local periodicity and infinite number of elements, the Floquet functions are obtained. These functions, describe the fields in terms of Fourier transformations and allow the reflectarray characterization taking into account the individual contribution of each element and the mutual coupling. Thus, it is possible to obtain the radiation pattern of each element within a periodic array environment, as well as the pattern of the whole reflectarray. Figure 13 illustrates a typical design of a reflectarray.

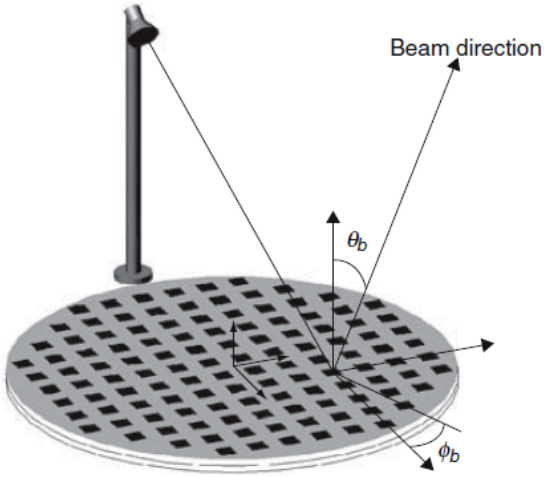

Figure 13: Printed reflectarray antenna example [13].

Despite of the subreflector is planar, it must keep the focus. Hence, the energy has to suffer a phase shift such that, it emulates the delay introduced by the conic curve. In other words, each individual array element located at (x_i, y_i) coordinate points, produces the same phase delay introduced by the **round trip** distance between the

planar surface and the original ADE curve. The subscript i notation express the individual element within an array of n number of elements. The application of this round trip theory is explained in chapter 3.1

The self-supported feed is designed such that a cylindrical horn antenna is attached to the ADE subreflector. This feed illuminates an AD Parabolic Reflector. Based on reflectarray technology, the ADE Subreflector is synthesised by means of rectangular patch cell phase shifters, resonant patches with variable size printed into microstrip substrate such as in Figure 28. The phase delay is implemented as is defined in the next Chapter 3 through the related mathematical and graphical support (Fig. 19).

2.4 State of the Art

Regarding the main objective and the scope of this work, the discussion of the state of the art presents the most relevant achievements on both, dual reflector antenna and self-supported feed systems in the scientific scenario. These sort of feeds are part of a dual reflector configuration which essentially is, a feed horn antenna with the subreflector attached by mean of a radome (Fig. 14). Thus, the fed system is supported by the mast of the horn, which is used to manage the signal from the transceiver. Therefore, the feed illuminates the attached subreflector and this, reflects the energy back to the paraboloid.

From the point of view of the global classification of a reflector antenna, this project aims to achieve a new technology able to illuminate a high gain reflector antenna, while it results into a low profile and competitive cost. This is made by means of modifying the classical dual reflector configuration in two aspects. The fed system, which is in charge of the primary radiation pattern, is composed by a self-supported printed subreflector which produces a ring focus radiation pattern in a reduced space. On the other hand, both reflectors are axially displaced geometry based, which prevents the blockage of the secondary radiation pattern due to the ring vertex.

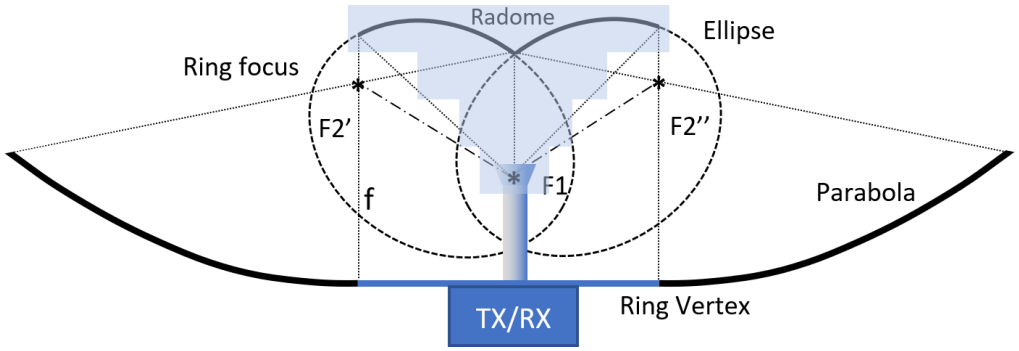

Figure 14: Subreflector attached to the self-supported feed horn antenna through a radome or dielectric.

Dual reflector configuration is the most compact geometry accordingly high gain reflector antenna. However, as is previously stated, there are build few Gregorian reflectors compared with Cassegrain systems [9]. Generally, reflectors may be cylindrical, spherical, as well as axi-displaced, axi-symmetric or distorted for customized radiation pattern. Even though there are several configurations types of sub and main reflectors, the blockage produced by the subreflector it is always present, as well as, struts shadows and feed support mechanism which complicates alignment and calibration. Offset dual reflector geometry prevents the blockage produced by the subreflector, although this increments cross polarization (XP). Both, blockage

and XP drawbacks are frequently solved by using axially symmetric geometries in both, reflector and subreflector surfaces. This are the classical Gregorian and Cassegrain configurations. Multiple sources have reported results regarding these systems [9, 15, 16, 17, 18, 19]. On October 2012 Milligan et al. presents a simple generalization of these sort of antennas [16] which has been used in this thesis. In 2013 the same author analyses the edge taper of SATCOM in X band in order to reduce side-lobes, which are often the weakness when matching with the measurement mask or template [17].

In the present work, the reference subreflector is an ADE surface. It means, the symmetry is no more in the axis but the ellipse is tilted. Thus, one of the foci is fixed and coincident with the feed. The second focus becomes duplicated due to the tilting. This aberration is denominated as astigmatism and it produces a ring focus feed. (Fig. 15). This sort of focus illuminates the main reflector with a ring shape. Therefore, a ring vertex surface is required, which is AD reflector [20].

AD reflectors have been proposed because of its inherent high aperture efficiency that derives in a particular advantage, the main reflector can be $\approx 20\lambda$ respect to classical arrangements such as Gregorian or Cassegrain. The classical configurations present less aperture efficiency because of the blockage produced by the subreflector. Due to the ray inversion produced by AD subreflectors the second focal point is out from the blockage area (Fig. 15). In 2009 it is reported an axially displaced reflector which provides 33.3 dBi at 8.484 GHz with an overall efficiency of 55% [21].

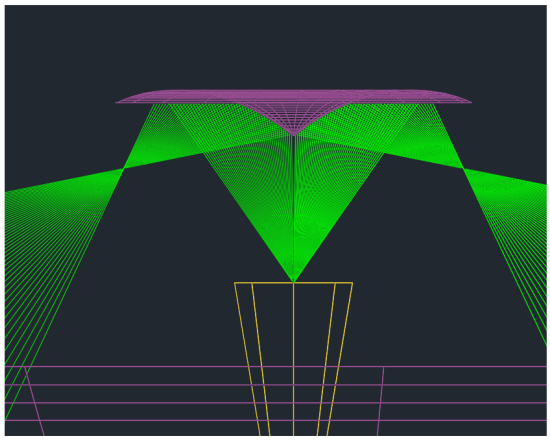

Figure 15: Ray inversion of axially displaced elliptical sub reflector producing ring focus.

That is to say, when displacing the axis of the main reflector, the vertex, previously a point, becomes a ring. Thus, the subreflector is not blocking the excitation area and it increases the effective aperture. Furthermore, this geometry produces low

reflection coefficient at the feed due to the out-coming rays, never return back into the feed from subreflector nor reflected back to this from the main reflector [19]. This idea is illustrated above in figure 15. All rays are dropped into the subreflector, this leads to a higher performance and more uniform illumination than Gregorian or Cassegrain systems [22, 18]. Although, the focal length to diameter (F/D) ratio of the main reflector results larger than in conventional designs, which means far-out side-lobes reduced, but higher profile of the antenna [22].

Additionally, the resultant subreflector is several times smaller, around $2\lambda - 4\lambda$, compared with those reported in Cassegrain systems. Moreover, AD reflector is compatible with dual-band feeds [23]. Self-supported fed system is based on circular waveguide (CWG) that acts as the mast of the feed. In addition, the subreflector is supported by a dielectric rod or a radome (Fig. 14). The dielectric can be also used to match the impedances [22]. The CWG may ends as conical horn to match the impedance progressively to the air. It supports infinite number of transversal TE and TM modes that in some applications, such as radar or tracking, are essential to create the symmetrical difference pattern [11]. However, the objective is to use the monomode bandwidth of the CWG. The existence of these propagation modes, depends mainly on the CWG diameter [24]. The fundamental mode TE_{11} produces relatively high level of cross polarization [25]. In case of **multimode** circular horn, because the TM_{11} mode has different phase velocity, it can be phased such that, the fundamental mode at the edges of the aperture is partially cancelled for E-plane [9]. Regarding **monomode** circular horn, this problem is compensated with chokes. It has been proved that using only one choke, the improvement is quite efficient [24, 26]. In this sense, the so called 'coffee can' design implements one single choke as main improvement. This artefact is coaxially reproduced several times in the aperture of Chaparral antenna for purifying linear polarization [27]. Therefore, chokes implementation reduce cross polarization as well as, side-lobe level [28] and equals the beam-width gathering phase centre of both E and H planes [29]. Additionally, for GNSS reference antenna system [30], chokes have been used to improve reception in low elevation angles of GPS and multipath rejection while not degrading other performance features.

Regarding the sub reflector component, Kildal presents in 1987 a Hat-fed system [31]. Despite this type of feed is initially proposed to reduce cross polarization, it has been applied to increase the efficiency in the sense of edge tapering decrement, side-lobes reduction and phase error compensation [32]. Dielectric material has been implemented for several reasons such as, matching adjustment of feed impedance, as well as in order to support the subreflector [22, 33, 34].

Chuan Liu et al. utilize polystyrene $\epsilon_r = 2.6$ and chokes on [22] as matching load, for reducing spillover and, due to the similarity between E-plane and H-plane, improve radiation patterns. Recently, much research has been devoted to improving the feed system in the line of the hat-fed. For instance, Erik G. et al. optimize the design through a commercial finite difference time domain (FDTD) solver by using a genetic

algorithm (GA) [33] in Ku-band. The design, presents low voltage standing wave ratio (VSWR), high gain, low side-lobe and low cross-polar levels. So that, from the design presented by Kildal [31] which provided 10% bandwidth and $\eta_{aperture} = 64\%$, Erik G. et al. design improves bandwidth to 33% and $\eta_{aperture} = 55\%$ with the aid of computational methods.

In terms of innovation and the current state-of-the-art, the antenna concept is based on the synthesis an ADE subreflector into a to self-supported feed, by means of phase shifters printed in microstrip. The maturity of reflectarray technology makes this possible and it is significant due to the cost of manufacturing and the performance. In addition, this method aims to achieve higher subtended angles by the subreflector, which is advantageous with respect to the regular ADE subreflector because they are limited in this sense to larger F/D. Therefore, the low profile is addressed as part of rendering the antenna less voluminous.

3 Design of reflectarray-based subreflector

This section presents the methodology followed to accomplish the reflectarray-based subreflector. Firstly, the creation of the reference feed model is described, which is a self-supported ring focus feed. The procedure is explained beginning with the analysis of the reference feed to the synthesis in the reflectarray subreflector. The geometry is illustrated starting from classical prime focus to the ring focus system. Secondly, the most important parameters are explained as well as the significance of these results. Next, the results of the feeds simulations are presented and discussed.

3.1 Design methodology

The methodology begins with the creation of the reference system and the analysis of its features as an antenna. The reference antenna system is the combination of a main reflector and a reference subreflector. The main reflector is an AD parabolic surface and the feed is a self-supported hat-fed subreflector working on 94 GHz. This hat-fed subreflector is already designed as an ADE surface with definite size, elliptical curve and tilt angle ϕ_0. The dimensions of the radome and the main reflector diameter are provided. For instance, the radome establishes the point where to locate the cut plane, at 2.48 mm from the lowest point of the elliptical curve. The diameter of the main reflector is 84 mm. The feed horn antenna is modelled as a Gaussian source of radiation. These constraints and parameters (Table 3.2.1) are introduced in a design and optimization Matlab set of scripts (DOMSS) to define the reference antenna system. This set is written by UPM in order to design and optimize dual reflector antenna systems. It is able to execute GRASP 8 to perform a PO analysis and to produce the radiation pattern computed by this method. By means of this set, the reference system geometry is produced, as well as the radiation pattern. The process is iterated until the antenna complies the requirements, such as a gain $\approx$ 37 dBi (Fig. 29).

I. Geometry This high gain antenna is produced with the geometries explained with the mathematical expressions published by T. Milligan and C. Granet [9, 15, 16, 35]. The geometry configuration of the antenna is shown in Figure 30. The feed is a self-supported hat-fed system with a subreflector attached with the shape of an axially displaced ellipsoid (Fig. 16). This corresponds with the reference (REF) feed system. horn antenna and the radome has been obviate to render the picture clearer, although they is depicted in Figure 14. The main reflector is an axially displaced parabolic reflector. Granet presents four options [35] to design an AD reflector. This case corresponds with displaced-axis Gregorian antenna with single offset presented as option number one in [35]. These configuration parameters are aligned with the antenna requirements and they are quantitatively described in the next section 3.2.1.

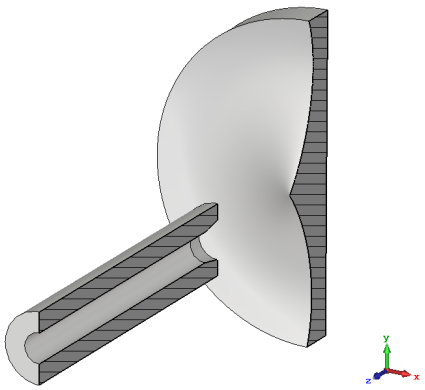

Figure 16: Reference ADE subreflector.

It has been incorporated to DOMSS two additional scripts. They analyse the phase delay introduced in the reflected E field by the reference subreflector. Then, the synthesis through reflectarray patch grounded cells is performed by means of multilayer reflect-array: design and analysis antenna tool from UPM (MRADANT-UPM). The reflectarray parameters (Table 3.2.1), as well as the cut plane in the REF subreflector where to locate the elements, are introduced in these scripts. They produce the phase delay computation and the subsequent phase-shit matrix required to produce the reflectarray mask.

II. Phase delay It is done by calculating the required phase-shift introduced by each element cell. The phase delay produced in the ray-tracing from the cut plane to the REF subreflector is computed. The phase-shift matrix corresponding the design parameters, such as number of cells or cell size, is produced (Fig. 21) and imported to MRADANT-UPM for the mask production. As is stated, the cut plane is defined by the radome, although it is adjustable at any point (Fig. 17). In this case, the objective is to remain the spike of the reference subreflector in order to simultaneously match the feed and to use an already designed radome .

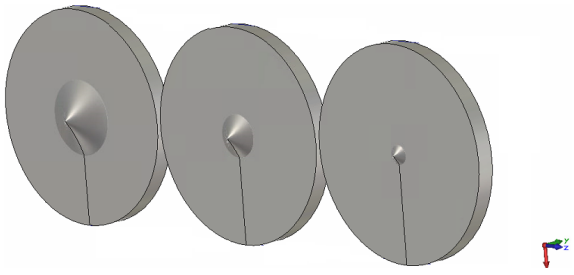

Figure 17: Three examples with different cut planes.

III. Round trip theory The feed horn antenna illuminates the reflectarray elements as in the case of a reflector. The elements of the reflectarray are tuned to produce a phase-shift on the incident field. For instance, it forms a planar phase front in the far field of the system when the synthesized surface is a paraboloid (Fig. 18). Therefore, the round trip path between the paraboloid and the reflectarray produces a phase delay in the incident field, which determines the wave front produced, hence the direction of the beam.

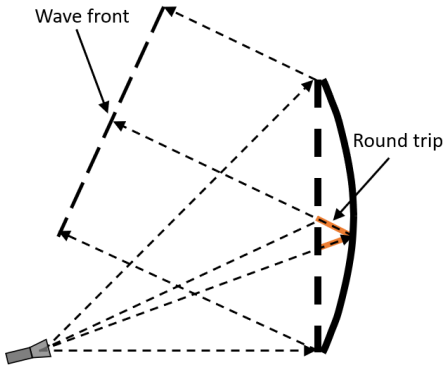

Figure 18: Planar wave front produced by a reflectarray equivalent to a parabolic reflector [13].

In the case of the REF subreflector the reflectarray is located at the cut plane. This is considered as the phase reference plane. The required phase-shift at each reflectarray element is the phase delay produced along the round trip path (Fig. 18). Thus, the incidence plane is represented in Figure 19 and it corresponds with $\varphi_{b_i} = 0°$.

The incident ray trip, in light red, starts in the focus *F1* and it ends on the REF curve.This distance is d_{inc} (mm). The ray is reflected in the direction of *F2* due to the properties of the ellipse; the sum of the distances from one point of the ellipse to the foci is constant. This distance is defined as d_{ref} (mm). The distance from the REF curve to the reflectarray (RA) plane is defined as d_{mid} (mm). The distance of the incident and reflected rays regarding the reflectarray are defined with apostrophe, d'_{inc}, d'_{ref} respectively.

Distances are computed through (x, y, z) coordinates. Those belonging to the reference (REF) curve are represented by (x_i, y_i, z_i) and regarding reflectarray (RA) points are represented as (x'_i, y'_i, z'_i). Note at the incidence plane of Figure 19 coordinates y_i and y'_i are zero. Also, at the cut plane, z' coordinate is constant.

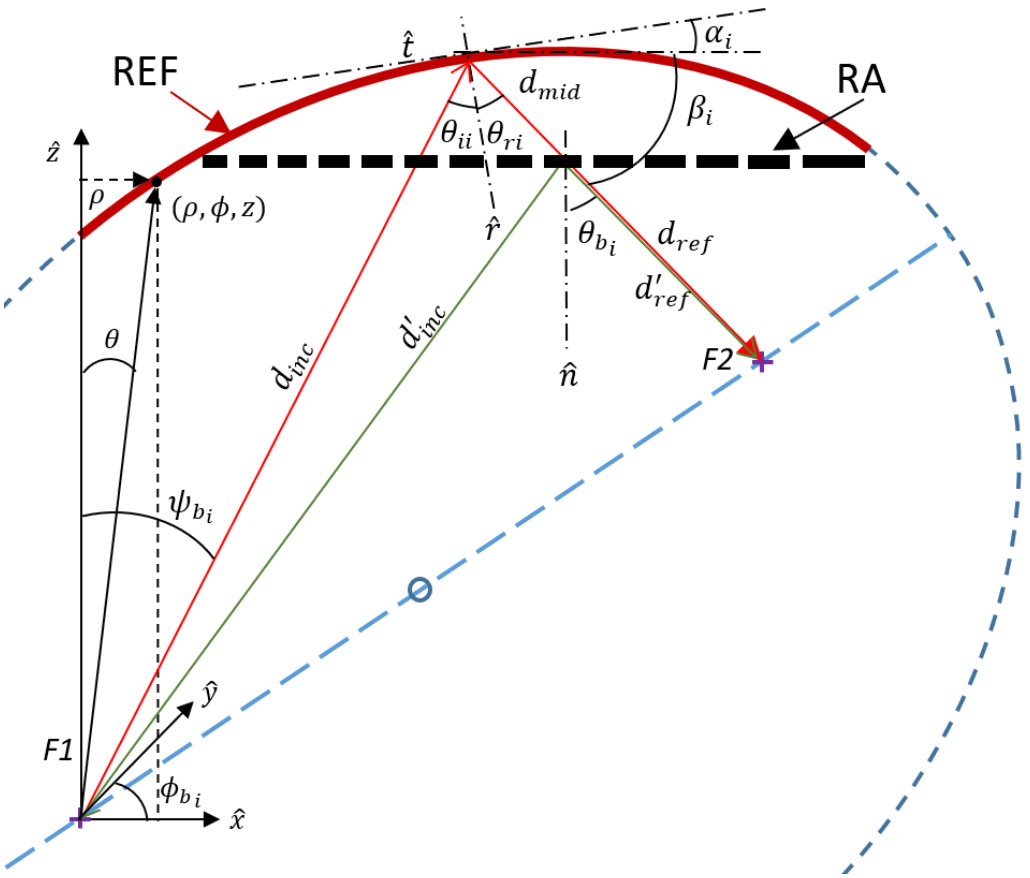

Figure 19: Ray-tracing for both ADE and RA curves.

Thus, due to the properties of the ellipse,

$$d_{inc} + d_{ref} = 2a \tag{3.1}$$

where $2a$ is the distance between foci. Phase delays are retards in the wavelength of both Electromagnetic (EM) fields

$$\Phi(x_i, y_i, z_i) = -k_0 d_{inc} - k_0 d_{ref} \tag{3.2}$$

where k_0 is the propagation constant in vacuum. In the case of the reflectarray, the elements shift the phase of the incident ray,

$$\Phi(x'_i, y'_i, z'_i) = -k_0 d'_{inc} - \Phi_R(x_i, y_i, z_i) - k_0 d'_{ref} \tag{3.3}$$

The reflected ray distance from REF is the distance of the sum of the middle distance in between the REF and RA and the reflected ray distance from RA.

$$d_{ref} = d'_{ref} + d_{mid} \tag{3.4}$$

By combining Equations (3.2), (3.3) and considering both $\Phi(x_i, y_i, z_i)$ and $\Phi(x'_i, y'_i, z'_i)$ equal.

$$\Phi_R(x'_i, y'_i, z'_i) = k_0(d_{inc} + d_{mid} - d'_{inc}) \tag{3.5}$$

where $d_{inc} + d_{mid}$ is the round trip distance.

$$d_{inc} = \sqrt{x_i^2 + y_i^2 + z_i^2} \tag{3.6}$$

$$d'_{inc} = \sqrt{x_i'^2 + y_i'^2 + z_i'^2} \tag{3.7}$$

where $z_i'^2$ is the position of the cut plane.

$$d_{mid} = \frac{z_i - z'_i}{\sin \beta_i} \tag{3.8}$$

The angle β_i is the angle of the reflected ray with respect to the $\hat{y}$ axis and it is defined as

$$\beta_i = \pi/2 - \theta_{b_i} \tag{3.9}$$

$$\theta_{b_i} = (\theta_{i_i} + \theta_{r_i}) - \psi_{b_i} \tag{3.10}$$

$$\theta_{i_i} = \alpha_i + \psi_{b_i} \tag{3.11}$$

$$\psi_{b_i} = \arctan\left(\frac{x_i}{z_i}\right) \tag{3.12}$$

where α_i is the angle of the tangent line $(\hat{t})$ at each point of the REF curve (x_i, y_i). The surface is considered as perfect electric conductor (PEC) then $\theta_{b_i} = 2\theta_{i_i} - \psi_{b_i}$.

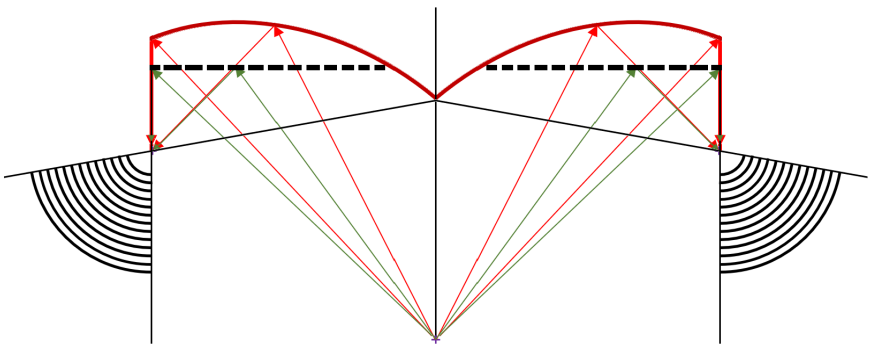

Figure 20: Spherical wave front produced by the ring focus of both, REF subreflector and the equivalent reflectarray.

Note when one ray strikes a planar PEC surface, by Snell's Law, it is reflected with the same incident angle with respect to the normal ($\hat{r}$) of the surface in that point (Fig. 19). Consequently, the family of rays out-coming from the focus *F1* would never converge on focus *F2*. Therefore, in order to focus the beam, the reflectarray introduces a required phase-shift($\phi_R(x_i', y_i', z_i')$) at each element of the grid to produce a shaped beam in the $(\theta_{b_i}, \psi_{b_i})$ direction.

The Equation (3.10) is related to the manipulation of the Snell's Law. Note that θ_{b_i} is the reflection angle produced by the REF curve, although this reflection angle is achieved by the reflectarray. Therefore, the incident angle ψ_{b_i} is now independent of the reflection angle θ_{b_i}.

The resulting phase delay from the calculations and the phase-shift matrix of the RA cells, are shown in Figure 21. Note from Equation (3.5) that at the spike, or central part of the reflectarray, $d_{mid} = 0$ and it has a delay of 0°because the path difference between REF and RA are the same in the spike.

As is mentioned, reflectarray technology is sensitive to the direction of the field, which makes it useful for polarisers implementation. It is also responsive to the frequency of the fields, thus it can perform a filter. However, the feature explored on this study is referred to the angle of incidence. Reflectarray allows to change the Snell law introducing phase changes on the reflected or transmitted fields. Therefore, the application of this reflectarray reminds to a lens because the phase shift is producing beam collimation. This technique is valid for transmitarray, where the main difference is the absence of the ground plane.

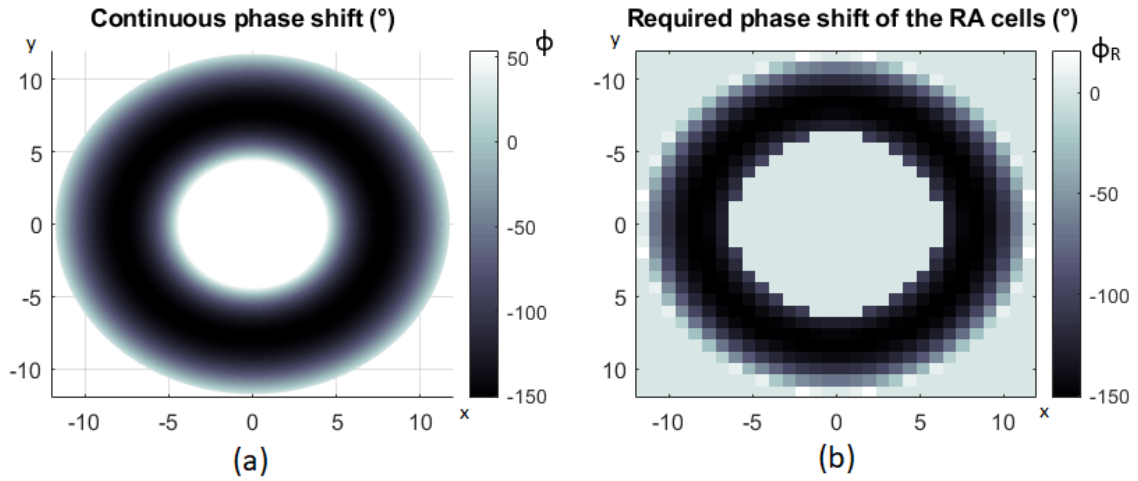

Figure 21: Phase delay of REF subreflector (a) and phase-shift matrix of the RA subreflector (b). x and y in mm, ϕ and ϕ_R in degrees.

IV. MRADANT-UPM The planar area surrounding the spike is divided in cells. These cells are filled by resonant patch printed elements, which perform a shift on the incident field phase. The required phase-shift introduced at each element produces a shaped beam [13]. The phase-shift matrix computed, as well as the rest of specifications (Table A1) are introduced in MRADANT-UPM software in the form of input files. However, the phase-shift matrix computed has an empty area in the centre, which contains the spike of the REF splashplate. For this reason, it is not possible to use the graphical user interface (GUI) (Fig. A1) and it is done by editing the input files. After to produce the preliminary files, the unit patch cell can be analysed. This is done by varying the size and the frequency (Fig. 23) to study the phase control.

It exists few parameters defined in the files, but not used. For instance, the ones related with radiation pattern representation, they need to be defined in the preliminary design files, but the radiation pattern function is not used. The analysis of the periodic array with ground plane is done by Method of Moments in spectral domain (MoM-SD) because of its efficiency and accuracy. The field reflected on each element is obtained by the product of the field and the reflection coefficient matrix, considering mutual coupling in one only periodic cell, Floquet's theorem [13]. The reflection coefficient matrix contains the fields scattered by the patches and the fields excited in the areas without patches.

V. Patch unit cell Once the phase matrix is analysed and the patch sizes are computed, it is possible to iterate the design the element cell such that the phase response satisfies the objective. For instance, enough bandwidth, low losses, low cross-polarization. The phase-shift of the patch element under analysis shows a linear response with the length (Fig. 23). The behaviour in both polarizations is the same. The analysis of Figure 21 verifies the capacity of this phase shifter to produce a phase shift in the range of 200°, which is the margin required (Fig. 21) to synthesize the REF REF splashplate. The control of the phase is done by varying the size of the patch cell w (Fig. 22) and it is performed by MRADANT-UPM.

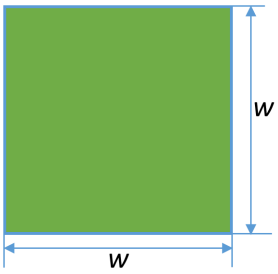

Figure 22: Patch cell size parameter.

Note that reflectarray cells are bigger than reflectarray patches, hence, the patches never touch each other. The parameters which configure the patch element are described in the Table 1. Additionally, the annex A shows the GUI of MRADANT and describes in the Table A1 all the parameters used in the synthesis.

NEX, NEY	Number of elements in X and Y axis	30	-
PX, PY	Periodic cell x,y dimension	0.8	mm
ANMIN	Minimum patch size	0.1	mm
ANMAX	Maximum patch size	0.78	mm

Table 1: Parameters of the reflectarray elements.

The main drawbacks of the resonant patch cell is the small bandwidth and the phase shift produced lower than 360°. As stated in section 2.3, this is solved by stacking elements in a multilayer reflectarray. The reflectarray cell is analysed in X and Y polarizations and both are identical,hence, only X polarization is shown in Figure 23.

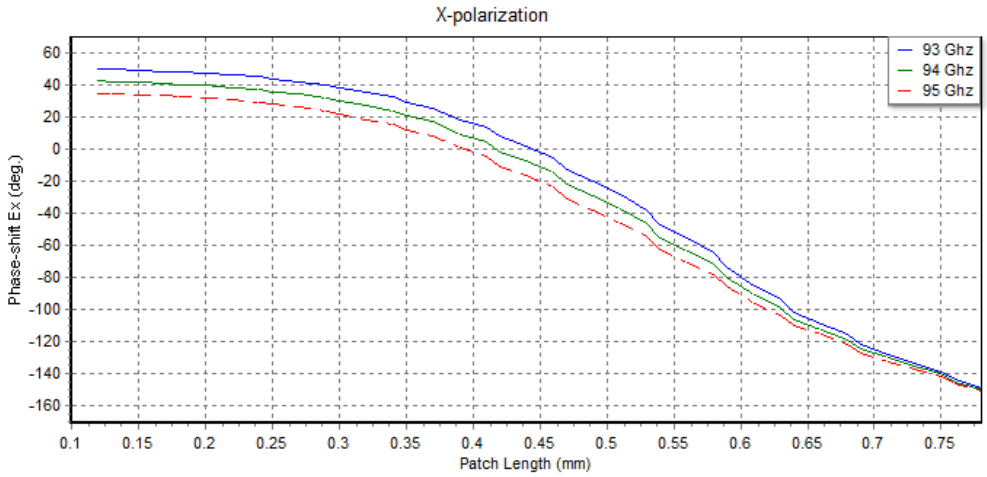

Figure 23: Phase shift (°) of the reflected E field in the patch cell with the size w (mm) in X-polarization.

Finally, MRADANT-UPM exports the mask in the form of an script (Fig. 24). This is introduced in AUTOCAD and the mask is transformed into a format that CST Microwave Studio is able to import.

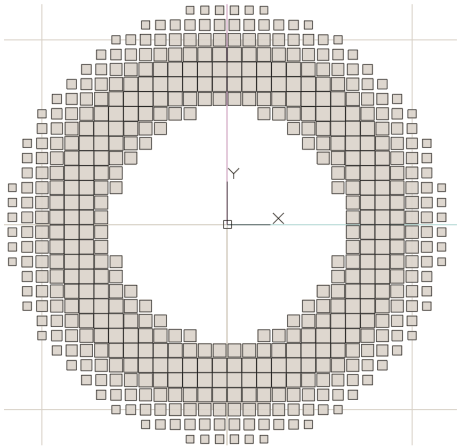

Figure 24: Reflectarray mask of RA subreflector.

VI. EM Simulation The synthesis is simulated in CST MS together with the feed horn antenna. The RA subreflector is created with the combination of the mask, the substrate and the spike from the REF subreflector (Fig. 25). The mask is reproduced in the 35 μm copper layer of the Arlon DiClad 880 substrate.

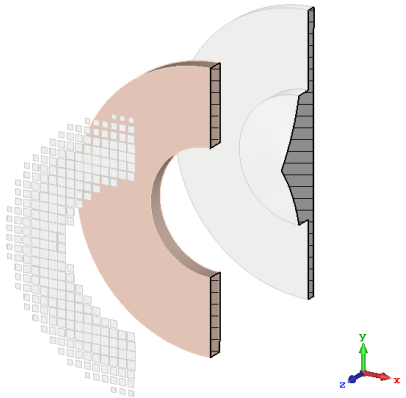

Figure 25: Reflectarray synthesis example. From left to right, mask pattern substrate

VII. Reference model Regarding the analysis of the RA feed (Fig. 28) two reference models have been taken into account. One of them, the (REF) ADE subreflector (Fig. 16), because it is the original model to be synthesized. The other model is a (full metal (FM)) full metal flat subreflector which only performs as hat-fed system with no phase shifters (Fig. 26). This model is used to show, in contrast, the effect of the phase shifters. It conserves the continuity of the metallic surface. The phase shifters are discrete and they leave areas in the substrate absent of metal.

Therefore, there are no induced currents and the energy can not be re-radiated. This design is absent of phase shifters and the curve is produced in the same manner as RA.

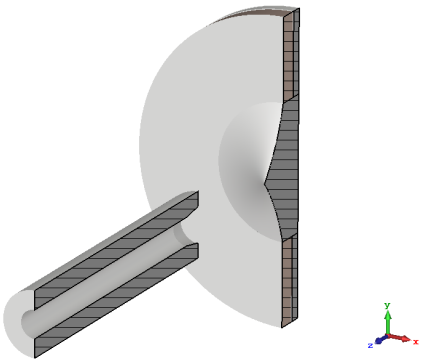

Figure 26: Full metal FM subreflector

VIII. EM Simulation The CST simulation has been configured to monitor the far field response of the feed, i.e. the radiation pattern. It is centred in 94 GHz with a span of 2 GHz. At central frequency, the λ=3,19 mm. The manufacturer of the software recommends a minimum of 10 mesh cells per wavelength, although in order to increase the accuracy these simulations have been set with 15 cells per wavelength. Considering applied the symmetry planes, this renders a mesh grid of 27.7M cells and with an steady time for the excitation at the level of -35 dB, the simulation lasts 24 hours.

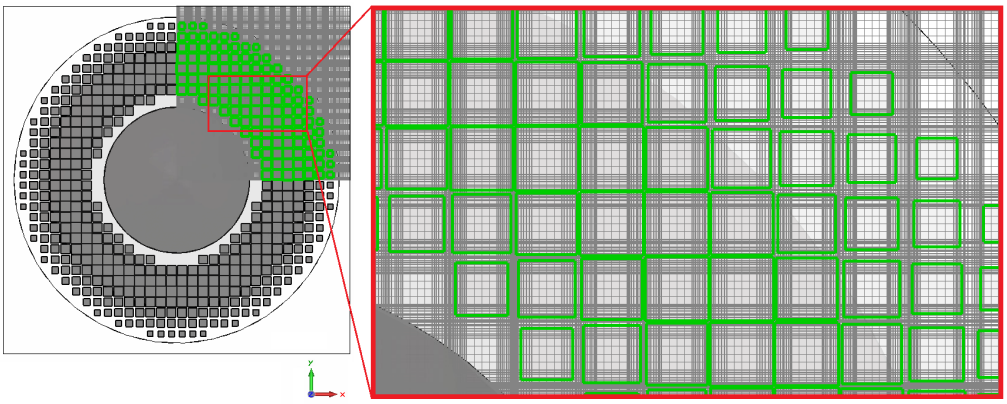

Figure 27: Mesh grid of RA subreflector

IX. Models The subreflector model curves, both the front and the rear, are cloud of points exported from DOMSS and imported to CST. These are transformed in curves which are axially sweep producing the metallic subreflector in few steps.

REF is built in Matlab through the DOMSS commented. This is fed by a horn antenna already designed at 94 GHz. The characteristics of this horn are exposed in chapter 3.2.2, however its CAD model is not authorized to be published, therefore the illustration shows a cropped horn antenna. After realizing the geometry and the CST simulation radiation pattern, the results expected are a ring shape behaviour on the radiation pattern, high gain in the ring focus angle and low reflection coefficient in the propagation modes TE_{11} y TM_{10} of the feed.

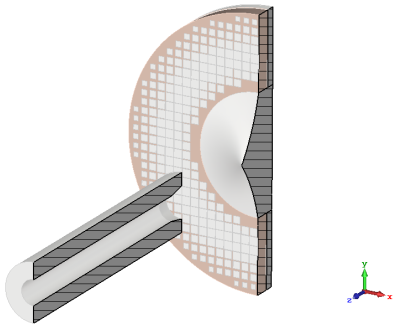

Figure 28: Reflectarray RA subreflector.

3.2 Results and discussion

Results chapter summarizes the outcomes obtained throughout the realization of this work. This chapter is organized in the following manner; the most important parameters and considerations regarding the results are previously introduced. Next, it continues with the characterization of the 94 GHz horn antenna that feeds the models under test: reference, full metal and reflectarray. Finally, results are presented regarding these three hat-fed systems. The evaluation of the feed results is done by comparison with the radiation pattern of all of them.

3.2.1 Parameters and features

The REF subreflector is validated within a full antenna system. This corroborates the subreflector as a valid starting point. This section briefly comments the parameters used on such validation.

First of all, the reference splashplate system is simulated when it is located at the designed point and it is moved such that the phase centre of the horn coincides with the focal point. Diameter of both sub and main reflector are imposed by design, in this case the main reflector diameter is 84 mm and the subreflector diameter is 23 mm. The diameter determines the directivity of the antenna for a specific value of efficiency η, which normally includes estimation of aperture-illumination efficiency, spillover losses and surface losses. Nevertheless, it does not include blockage produced from struts because this structure is based on self-supported feed. Since it is an AD reflector, the effective area of the aperture is the area of the paraboloid. However, the total size of the antenna is increased due to the "hole" produced by the axis displacement, which corresponds with the subreflector diameter. The polarization of the feed is linear in the $\phi = 90°$ plane, hence, the antenna system is linearly polarized. It is measured in the band of [92-96] GHz with 94 GHz as central frequency. The bandwidth is given in percentage for level of $S_{11} \leq -20dB$. The focal length to diameter f/D ratio is 0.4, which corresponds with 78°of subtended angle of the feed in the optimized main reflector model used for REF feed. Table 3.2.1 specifies the value of each parameter of the REF design. These are referred in Figure 30. The maximum gain of the aperture antenna assuming 100% efficiency due to the absence of blockage.

$$D(dB) = 20\log\left(\frac{\pi D_m}{\lambda}\right) = 38.35dB \tag{3.13}$$

The antenna system described is introduced in GRASP 8 for PO analysis. The feed of the REF subreflector is modelled as a linearly polarized gaussian feed with -20 dB edge taper at 46°. The radiation pattern of the whole antenna system is given

below in Figure 29. This result validates the geometry of the main and sub reflectors. Therefore, the subreflector is correct to be simulated in CST Microwave Studio in order to obtain the REF radiation pattern, which is the model to be synthesized.

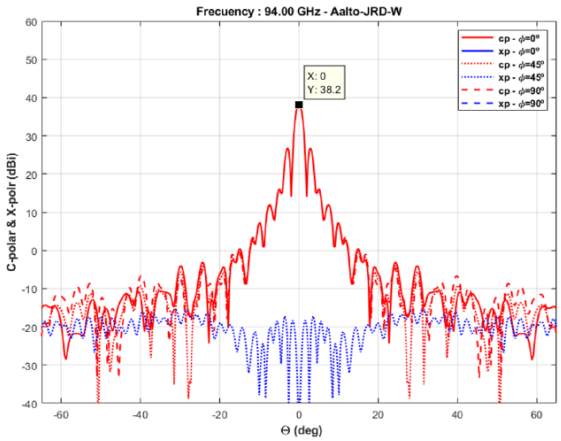

Figure 29: Radiation pattern of the reference antenna system.

Parameter	Description	Value	Units
D_{mr}	Main parabolic reflector diameter	84	mm
F/D	Focal distance to Main reflector diameter	0.4	mm
Lm	Feed to Main reflector vertex distance)	8.3	mm
D_{sr}	REF subreflector diameter	23	mm
Ls	Feed to Subreflector vertex distance	11.6	mm
ϕ_0	Ellipse tilt angle	76.6	°
ϕ_S	Subreflector edge	44.8°	mm
ϕ_M	Half-subtended angle	78	°

Table 2: Geometrical parameters of the Axially Displaced reflector system

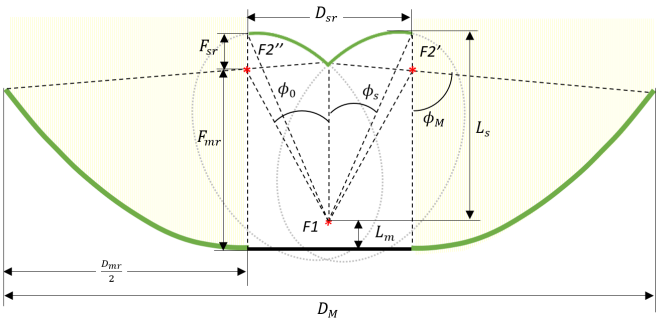

Figure 30: Antenna system geometry with REF subreflector. Not real proportions.

The radiation pattern of the feed must be committed with the shape of the ring focus. However, it must be taken into account that exist induced currents on the mast of the horn, which radiates contributing to the energy radiated towards $\theta = 0$. Furthermore, the feed is self-supported with a mast connected to the paraboloid, hence, on the base of the mast there is a large metallic surface. This is simulated through disk plate located at the port. In addition, another disk is located in order to cancel the induce currents on the mast, as stated on the state-of-the-art these artefacts are called chokes. The distance between disks has to be $\lambda/4$. It is $\approx 70\%$ the size of the subreflector and it simulates the vertex of the main reflector partially cancelling the induced currents on the mast. The choke is shown in Figure 31. The impact over the radiation pattern of the feed is illustrated in Figure 32.

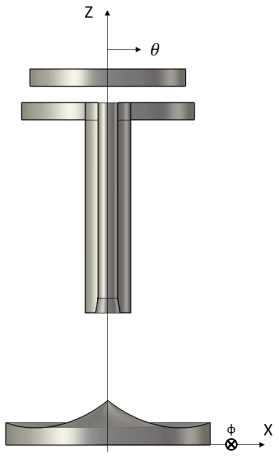

Figure 31: Choke implementation at the base of self-supported feed.

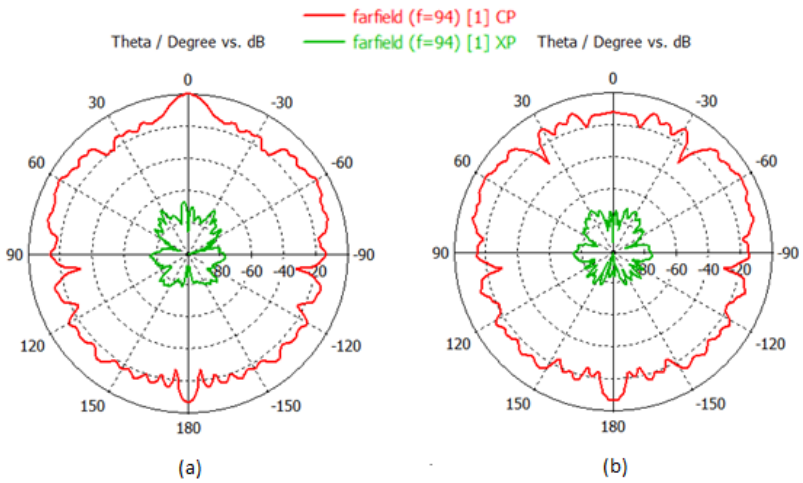

Figure 32: Copolar and crosspolar radiation patterns of REF subreflector without choke (a) and with it (b) ($\phi = 0$).

One of the electrical characteristics that must be verified after the simulation is the standing wave ratio (SWR), or the equivalent S_{11} (dB), illustrates the matching response in the desired band. This step must be done for the two orthogonal TE_{11} modes generated on the CWG. Additionally, the third mode TM_{01} needs to be checked. The matching is eminently related with the feed horn antenna used for illuminating the subreflector. Next section describes the horn.

3.2.2 Feed horn antenna

An optimized 94 GHz feed horn has been used for illuminating the subreflectors designed. As well as, it has been used in the analysis of the excitation port modes generated on it. These ports have to be taken into account in the design process. The waveguide port excites the CWG and several modes can be produced at the operation bandwidth depending on the internal radius of the CWG. This CWG used for illuminating the subreflectors designed has an internal diameter of 2.26 mm. It allows the propagation of the two first modes between the frequencies 77.78 GHz and 101.62 GHz. The following expression from [25] determine these frequencies.

$$f_{c_{mn}} = \frac{k_c}{2\pi\sqrt{\mu\epsilon}} = \frac{p'_{nm}}{2\pi a\sqrt{\mu\epsilon}} \tag{3.14}$$

where p'_{nm} is the mth root of the derivative of J_n which is the Bessel function.

n	p'_{n1}	p'_{n2}	p'_{n3}
0	3.3832	7.016	10.174
1	1.841	5.331	8.536
2	3.054	6.706	9.970

Table 3: m^{th} root of the derivative of the Bessel function.

The first TE mode, which belongs to the smallest p'_{nm}, is the dominant mode of the CWG, and it is the most frequently used. Note that $m \geq 1$ thus, there is not TE_{10} and in those cases where $m = 1$ two orthogonal modes are propagating at the same time [25]. These two orthogonal modes, TE_{11}, plus the third, TM_{10}, are analysed at the feed horn. As it is shown in Figure 33, (1) and (2) responses are both TE_{11} orthogonal modes. The TM_{10} mode is represented as (3). Thus, it is proved that the feed horn antenna does not propagate TM_{10} mode in the operation band. Therefore, only TE_{11} mode is simulated henceforth. Only one of the two orthogonal modes is

simulated because the other is cancelled due to the boundary conditions applied in the CST simulation.

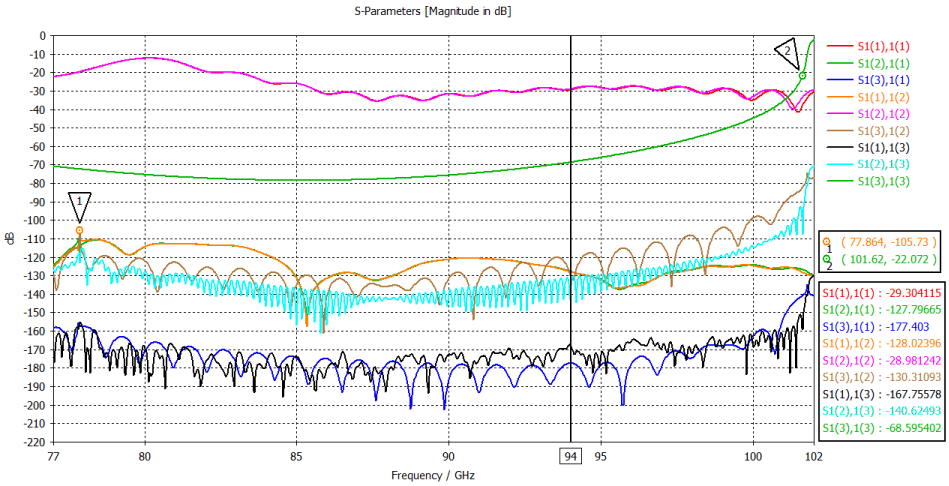

Figure 33: S11 parameter of the first three propagation modes on the W band feed horn antenna.

The radiation pattern of the feed horn antenna allows to compute part of the contribution to the edge taper, which is -10 dB at $\theta_{max} = 43.36°$. This is ψ_0 angle at equation (2.20).

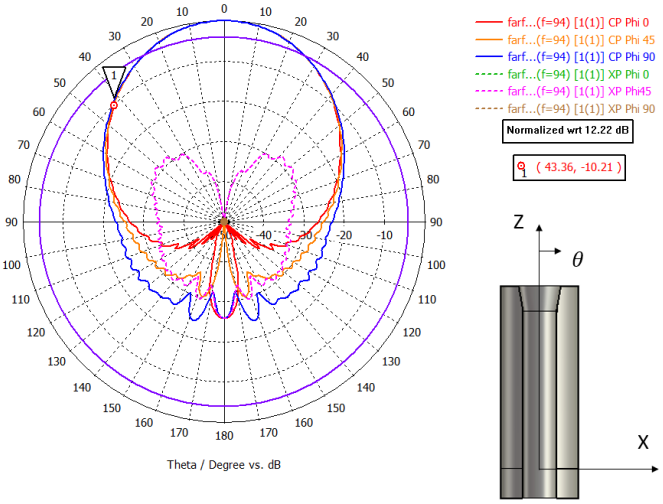

Figure 34: Radiation pattern of W band feed horn antenna. Normalized with respect to 12.22 dB.

3.2.3 Feed system results

This chapter presents the outcomes of the feeds. These are presented in the form of the S_{11} parameter and far field results comparison between REF, RA and FM. Firstly, the matching level of the feeds are satisfactory (Fig. 35).

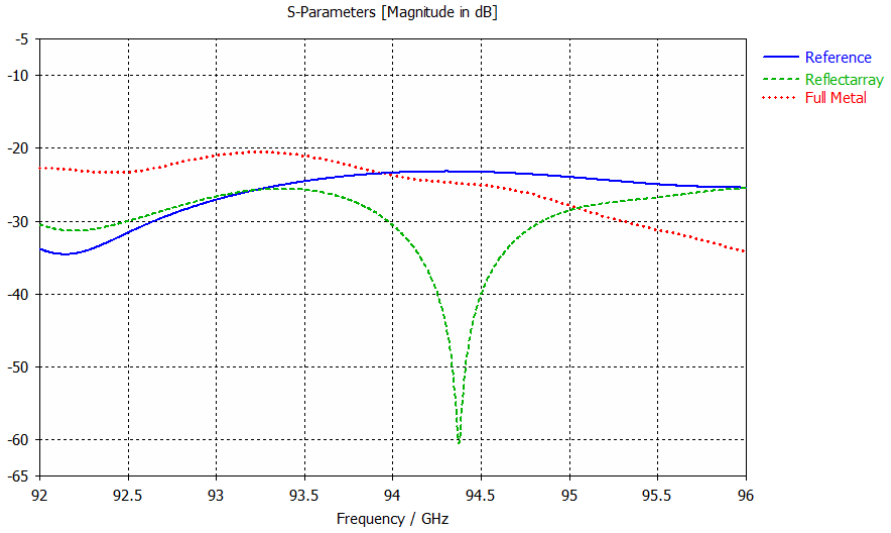

Figure 35: S_{11} parameters of the feeds simulated.

The radiation pattern of the reference feed (REF), the full metal feed (FM) and the reflectarray synthesis feed (RA) is shown in polar form in Figure 36. The performance of the synthesized subreflector is evaluated with respect to the reference feed, as well as with the full metal. Thus, the feeds present three main radiation zones (Fig. 37) where the behaviour of the reflectarray is analysed by contrast with the full metal.

The first zone (Fig. 38) is where the reflectarray is dominant. Due to the inversion of the rays, this zone is more contributed by the reflectarray and compared with full metal, the patches perform accordingly to the reference pattern. Therefore, there is a right agreement between reflectarray and reference phase behaviour.

In the second zone (Fig. 39), the spike belonging to the reference subreflector, contributes more to the radiation and it is the ring focus direction. However, reflectarray presents a discordance in plane $\phi = 0°$ at 53°. This reduces the illumination efficiency of the main reflector, due to the radiation is not uniform in the ring vertex. It can be produced by the induced currents of the mast. This currents can be cancelled by implementing multiple $\lambda/4$ chokes in along the mast.

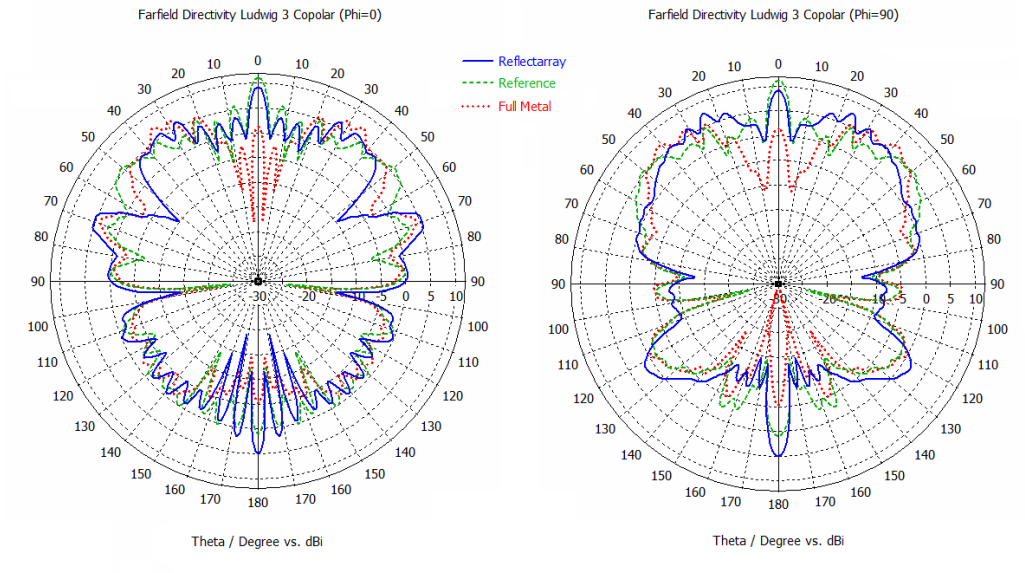

Figure 36: Radiation pattern of the reflectarray synthesis (RA). H plane ($\phi = 0°$) on the left hand side and E plane ($\phi = 90°$) on the right hand side.

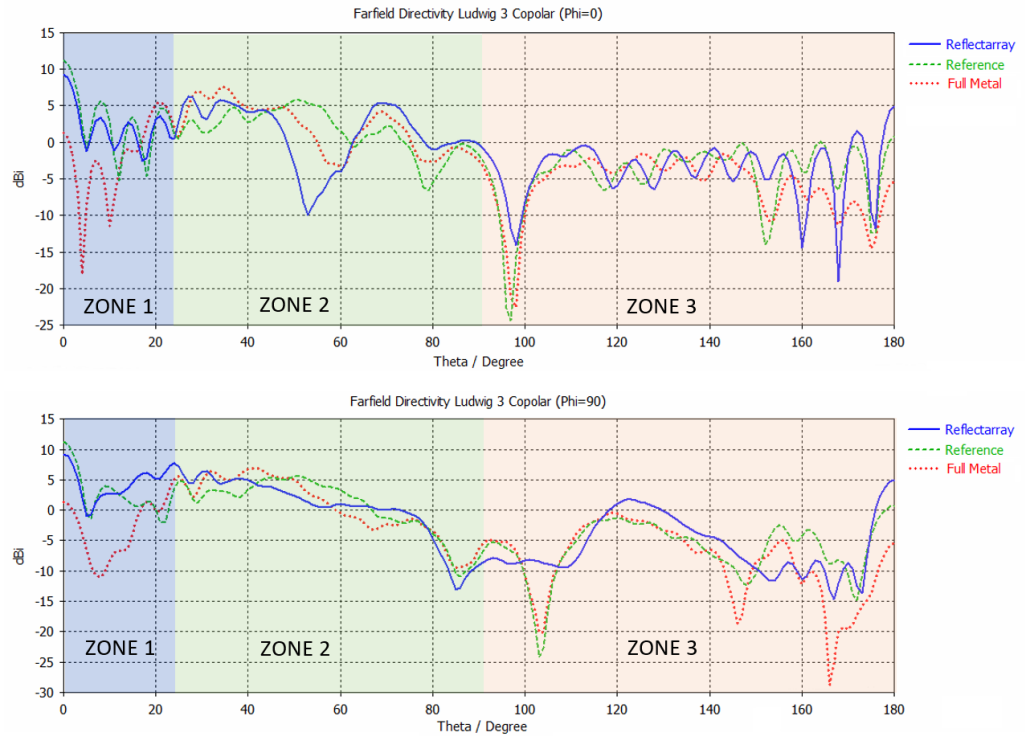

Figure 37: Radiation pattern of the three feeds simulated. H plane ($\phi = 0°$) at the top and E plane ($\phi = 90°$) at the bottom.

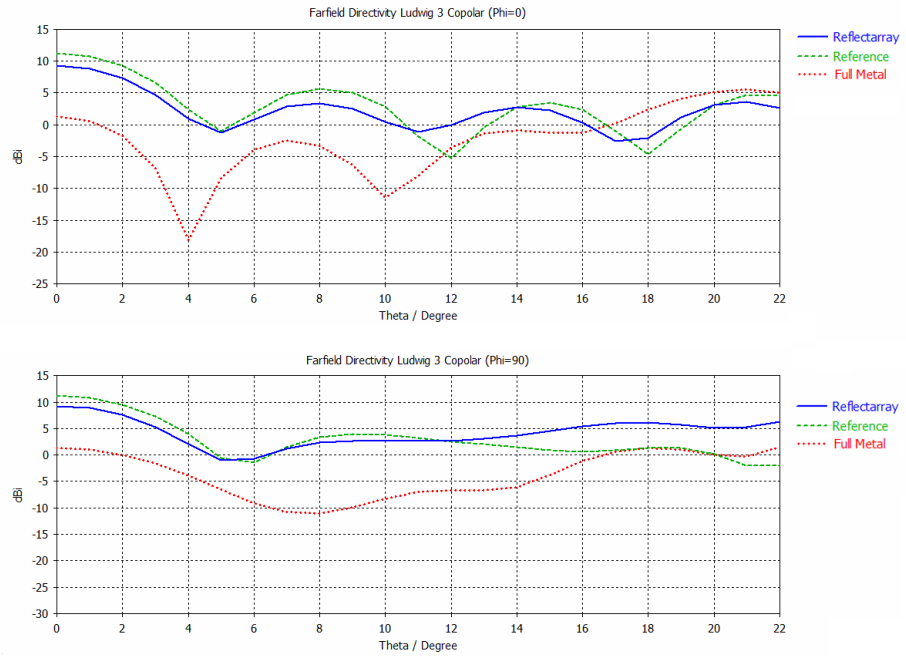

Figure 38: Zone number 1 of the radiation pattern comparative. H plane ($\phi = 0°$) at the top and E plane ($\phi = 90°$) at the bottom.

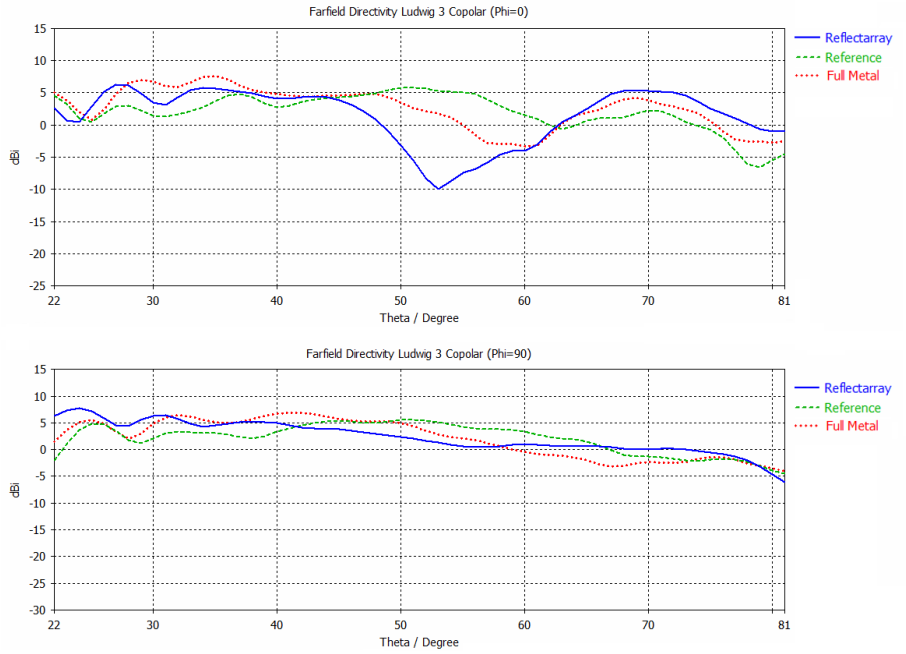

Figure 39: Zone number 2 of the radiation pattern comparative. H plane ($\phi = 0°$) at the top and E plane ($\phi = 90°$) at the bottom.

In the third zone the back side of the feed is represented (Fig. 40). Reflectarray produces higher back radiation and it is noticeable the correction of the null that the reflectarray performs at 103°of the E plane, although it is not symmetric.

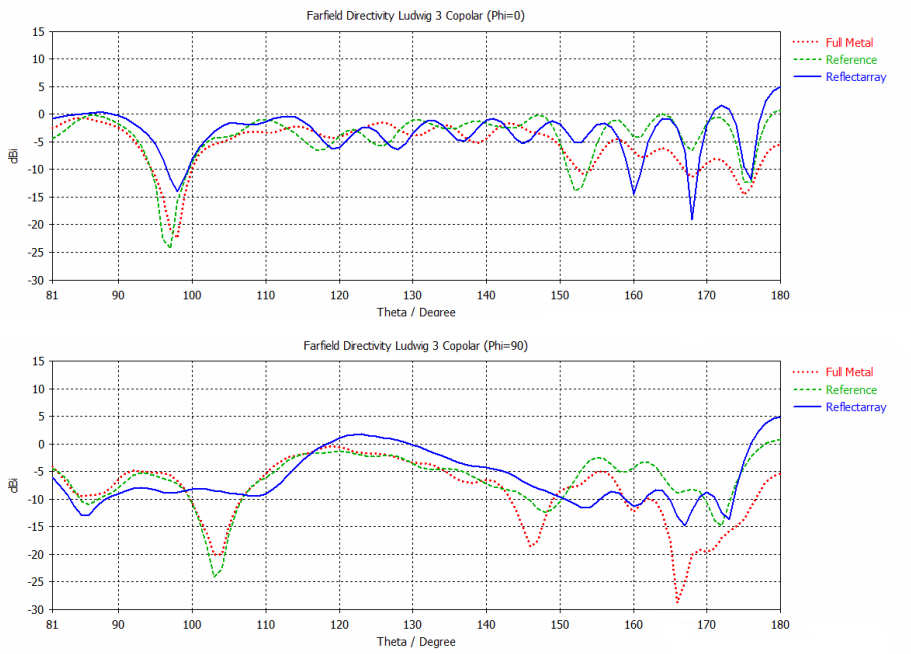

Figure 40: Zone number 3 of the radiation pattern comparative. H plane ($\phi = 0°$) at the top and E plane ($\phi = 90°$) at the bottom.

4 Conclusions and future lines

This chapter presents a summary of conclusions obtained from the results presented. As stated in the previous chapter, the geometry employed for the reference subreflector is validated as part of a high gain antenna system. Considering the similarity found in the radiation performance, the reflectarray synthesis could be substituted by the subreflector in the afore-mentioned high gain antenna system. Therefore, the presented results demonstrate the feasibility of the method by reducing costs, weight and size.

First of all, the mathematical assumptions have been corroborated and correctly translated to the phase matrix. The reflectarray feed produces a ring-shaped beam with similar characteristics to the reference feed. Despite the design methodology of the feed being validated, it requires further development. There is a noticeable discrepancy on the radiation pattern of the reflectarray located in 53°of $\phi = 0$ (H plane). It can be produced by a low phase resolution in the reflectarray synthesis. By increasing the number of cells, which is currently set to 30x30, it would lead to a more accurate current distribution. In other words, the minimum phase shift step between two adjacent cells might be sufficiently large to decrease the fidelity of the phase front reproduction. Therefore, by increasing the number of patches or reducing the maximum cell size, the phase-shift matrix of the reference subreflector would be more faithfully reproduced. In addition, the complexity of the manufacturing process is not affected, since it is fabricated by a regular photo-etching process.

One drawback is that resonant patch cells require a high density of mesh grid in the CST simulation. The computational method, used by the time domain solver to analyse the feed, is highly costly and limits the feed optimization procedure. Nevertheless, the simulations of the feed can be improved by implementing mesh grid groups in the CST simulation. For instance, the feed horn surrounded by the mesh cells (yellow squared area in (Figure 41) is computed with an oversized grid constrained by the object with the minimum size. Such a degree of accuracy is not necessary, because the objects are larger than the patches. Therefore, in the case of simulating with CST, it is recommended that mesh grid groups and/or mesh refinement are implemented to optimize the simulation

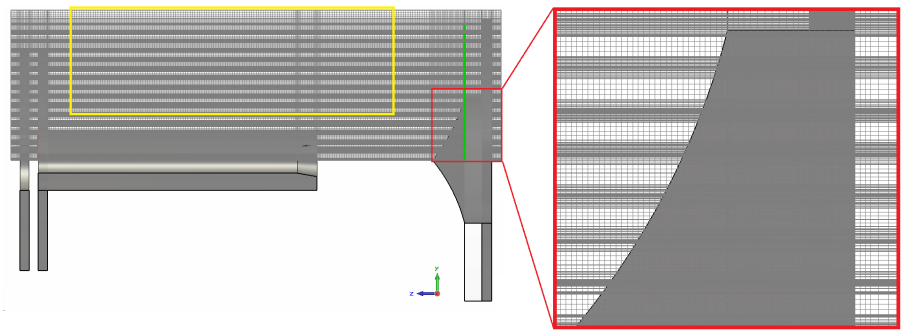

Figure 41: Longitudinal mesh grid of the feed.

Furthermore, in addition to the time domain solver of CST, more efficient analysis techniques could be used for the reflectarray, such as the Method of Moments in Spectral Domain, assuming local periodicity, which has been implemented in MRADANT-UPM. Additionally, symmetric phase shifters could be investigated in order to improve the symmetry of the radiation pattern. For instance, the concentric rings (Fig. 42), printed in the microstrip surrounding the spike of the subreflector, have been tested by the author as a promising phase shifter.

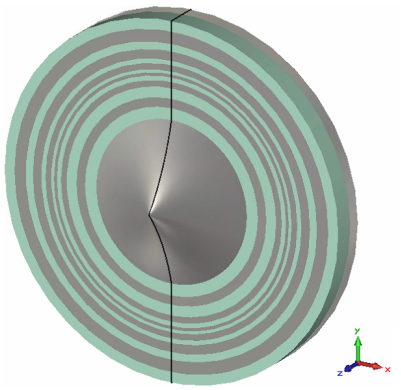

Figure 42: Longitudinal mesh grid of the feed.

To summarise, the reflectarray synthesis by resonant patches is successfully applied to the subreflector. Thus, the objective of the thesis has been achieved, the cost of the reflector is reduced, as well as the weight of the feed by implementing this reflectarray-based subreflector. However, the profile of the subreflector under synthesis is slightly reduced, due to the proximity of the tilt angle (ϕ_0) to 90 °. In this case $\phi_0 = 76.6$ °, which renders a shallow ADE subreflector. For instance, in the case of an ADE subreflector with a low ϕ_0 angle used to illuminate main reflectors with a smaller diameter, this method could considerably reduce the thickness of the subreflector, hence, the profile of the whole antenna.

References

[1] Miguel A. Salas-Natera, Ramón Martínez Rodríguez-Osorio, Leandro de Haro Ariet and Miguel Calvo Ramón, "Analytical expressions for the evaluation of gravity distortion impact on the antenna efficiency applied to large antenna uplink arrays," *IET Microwaves, Antennas & Propagation*, Nov 2017.

[2] M. A. Salas-Natera and R. M. Rodriguez-Osorio, "Analytical evaluation of uncertainty on active antenna arrays," *IEEE Transactions on Aerospace and Electronic Systems*, vol. 48, no. 3, pp. 1903–1913, July 2012.

[3] T. N. M. Sabbadini. European Space Agency. Noordwijk. Antenna design for space applications. [Online]. Available: http://www.uniroma2.it/didattica/ap2/deposito/Day_1.pdf

[4] G. Rubio-Cidre, C. Rodríguez, M. Ramírez-Torres, J. Grajal, and O. Rubiños, "Understanding cloud dynamics using a ground-based radar at 94 ghz," in *2017 IEEE Radar Conference (RadarConf)*, May 2017, pp. 1137–1141.

[5] C. Sanchis-Borrás, M. T. Martínez-Inglés, J. M. Molina-García-Pardo, J. P. García, and J. V. Rodríguez, "Experimental study of mimo-ofdm transmissions at 94 ghz in indoor environments," *IEEE Access*, vol. 5, pp. 7488–7494, 2017.

[6] M. S. Castañer, J. I. G. Fuertes, J. M. S. G. de Olea, R. M. Gallego, and J. L. F. Jambrina, "Radial line slot antenna design for monopulse space debris radar," in *2016 10th European Conference on Antennas and Propagation (EuCAP)*, April 2016, pp. 1–4.

[7] Á. Aznar, L. Roca, and S. Boris, *Antenas*, ser. Politecnos Series. Universitat Politècnica de Catalunya, 2002. [Online]. Available: https://books.google.es/books?id=AlQ8p2C4sCoC

[8] K. Pontoppidan, *Technical description for GRASP 8*, TICRA Engineering Consultants, Copenhagen, Denmark, 2002.

[9] T. Milligan, *Modern Antenna Design*, ser. Wiley - IEEE. Wiley, 2005. [Online]. Available: https://books.google.es/books?id=PPyDQXAd09kC

[10] C. Hitz, J. Ewing, and J. Hecht, *Introduction to Laser Technology*. Wiley, 2012. [Online]. Available: https://books.google.es/books?id=l3FKqoBLgNkC

[11] C. Balanis, *Antenna Theory: Analysis and Design*, ser. Antenna Theory: Analysis and Design. John Wiley & Sons, 2005, no. v. 1. [Online]. Available: https://books.google.es/books?id=agWwQgAACAAJ

[12] W. Stutzman and G. Thiele, *Antenna Theory and Design*, ser. Antenna Theory and Design. Wiley, 2012. [Online]. Available: https://books.google.es/books?id=xhZRA1K57wIC

[13] J. Huang and J. Encinar, *Reflectarray Antennas*, ser. IEEE Press Series on Electromagnetic Wave Theory. Wiley, 2007. [Online]. Available: https://books.google.es/books?id=JNwYCzFt8Z0C

[14] P. J. B. Clarricoats and G. T. Poulton, "High-efficiency microwave reflector antennas - a review," *Proceedings of the IEEE*, vol. 65, no. 10, pp. 1470–1504, Oct 1977.

[15] C. Granet, "Designing axially symmetric cassegrain or gregorian dual-reflector antennas from combinations of prescribed geometric parameters," *IEEE Antennas and Propagation Magazine*, vol. 40, no. 2, pp. 76–82, Apr 1998.

[16] N. R. Khachatryan and R. V. Ter-Antonyan, "Generalized dual- reflector axisymmetric antennas [antenna designer's notebook]," *IEEE Antennas and Propagation Magazine*, vol. 54, no. 5, pp. 162–171, Oct 2012.

[17] T. Milligan, C. Granet, J. S. Kot, and I. M. Davis, "Setting subreflector edge taper in a satcom dual-reflector antenna [antenna designer's notebook]," *IEEE Antennas and Propagation Magazine*, vol. 55, no. 6, pp. 128–136, Dec 2013.

[18] F. J. da Silva Moreira and J. R. Bergmann, "Axis-displaced dual-reflector antennas for omnidirectional coverage with arbitrary main-beam direction in the elevation plane," *IEEE Transactions on Antennas and Propagation*, vol. 54, no. 10, pp. 2854–2861, Oct 2006.

[19] S. R. Zang and J. R. Bergmann, "Omnidirectional dual-reflector antennas for flexible coverage," *IEEE Antennas and Wireless Propagation Letters*, vol. 12, pp. 821–824, 2013.

[20] J.-M. Wu, X. Lei, D.-f. Zhou, L. Hou, and H.-w. Chen, "Design of ring-focus elliptical beam reflector antenna," vol. 2016, pp. 1–7, 02 2016.

[21] C. Kumar, V. V. Srinivasan, V. K. Lakshmeesha, and S. Pal, "Performance of an electrically small aperture, axially displaced ellipse reflector antenna," *IEEE Antennas and Wireless Propagation Letters*, vol. 8, pp. 903–904, 2009.

[22] C. Liu, S. Yang, and Z. Nie, "Design of a parabolic reflector antenna with a compact splash-plate feed," in *2013 Cross Strait Quad-Regional Radio Science and Wireless Technology Conference*, July 2013, pp. 241–244.

[23] J. C. Lee, "The development, variations, and applications of an ehf dual-band feed," vol. 4, pp. 61–79, 01 1991.

[24] A. Kumar, "Reduce cross-polarization in reflector-type antennas," *Microwaves*, vol. 17, pp. 48–51, Mar. 1978.

[25] D. Pozar, *Microwave Engineering*. Wiley, 2004. [Online]. Available: https://books.google.es/books?id=4wzpQwAACAAJ

[26] G. L. James, "Radiation properties of 90° conical horns," *Electronics Letters*, vol. 13, no. 10, pp. 293–294, May 1977.

[27] P. W. W. (ex N1BWT), "Feeds for parabolic dish antennas," in *The W1GHZ Online Microwave Antenna Book*, 1994-2009.

[28] R. E. Collin and H. W. Schilling, "Dual-mode coaxial feed with low crosspolarisation," *Microwaves, Optics and Antennas, IEE Proceedings H*, vol. 131, no. 6, pp. 405–410, December 1984.

[29] P. D. Potter, "Horn antenna with suppressed sidelobes and equal beamwidth - radiation characteristics of dual - mode conical horn," JPL, Tech. Rep., feb 1963.

[30] W. Kunysz, "A three dimensional choke ring ground plane antenna," 04 2018.

[31] P. S. Kildal, "The hat feed: A dual-mode rear-radiating waveguide antenna having low cross polarization," *IEEE Transactions on Antennas and Propagation*, vol. 35, no. 9, pp. 1010–1016, Sep 1987.

[32] M. Yousefnia, A. Pirhadi, and M. Hakkak, "Analysis and design of parabolic hat feed antenna," in *2005 IEEE Antennas and Propagation Society International Symposium*, vol. 3A, July 2005, pp. 650–653 vol. 3A.

[33] E. G. Geterud, J. Yang, T. Ostling, and P. Bergmark, "Design and optimization of a compact wideband hat-fed reflector antenna for satellite communications," *IEEE Transactions on Antennas and Propagation*, vol. 61, no. 1, pp. 125–133, Jan 2013.

[34] E. G. Geterud, J. Yang, and T. Östling, "Wide band hat-fed reflector antenna for satellite communications," in *Proceedings of the 5th European Conference on Antennas and Propagation (EUCAP)*, April 2011, pp. 754–757.

[35] C. Granet, "A simple procedure for the design of classical displaced-axis dual-reflector antennas using a set of geometric parameters," *IEEE Antennas and Propagation Magazine*, vol. 41, no. 6, pp. 64–72, Dec 1999.

[36] W. Menzel, M. Al-Tikriti, and R. Leberer, "A 76 ghz multiple-beam planar reflector antenna," in *2002 32nd European Microwave Conference*, Sept 2002, pp. 1–4.

[37] E. M. M. de Rioja del Nido, "New advances on multi-frequency and multi-beam reflectarrays with application to satellite antennas in ka-band," 2018. [Online]. Available: http://oa.upm.es/50302/

[38] A. P. Popov and T. Milligan, "Amplitude aperture-distribution control in displaced-axis two-reflector antennas," *IEEE Antennas and Propagation Magazine*, vol. 39, no. 6, pp. 58–63, Dec 1997.

A MRADANT-UPM parameters

Parameters	Units	Description
xf, yf, zf	mm	Coordinates of feed position.
NEX, NEY	m	Number of elements in X and Y axis.
THETA0X, PHI0X, THETA0Y, PHI0Y	°	Angle of the radiated beam for X and Y polarizations.
PX, PY	mm	X and Y dimensions of the periodic cell.
F0, DF, NF	Hz	Central frequency, increment of frequency and number of points.
NH, NS, NBF, CNTE	-	Relatex with Floquet harmonics for Method of Moments.
ANMIN, ANMAX, NPOINTS	mm	Minimum and maximum dimensions of patches.
NPOINTS	-	Number of points for the phase curve.
TSUB, ERSUB_Real, ERSUB_Imag	-	Substrate properties. Thickness and complex permitivity.
TSUP, ERSUP_Real, ERSUP_Imag	-	Superstrate properties. Thickness and complex permitivity.
NL	-	Number of layers (1, 2 or 3)
ALPHA1, TS1, ER1Real, ER1Imag	-	Relative factor to the first layer. Substrate properties of the first layer.
NF0, CTE1,C2	-	Constant to fix the origin point for phase distribution.
CTE1	°	Constant added to the phase-shift of the reflectarray element.
C2	°	Constant to adjust the phase difference at extreme frequencies.
QF		Quality factor.
UMIN, UMAX, VMIN, VMAX, SRP, MINRP	°	Extreme values of the u and v angular coordinates for the radiation patterns. Not used.
EFF	-	Estimated antenna efficiency to evaluate the directivity.
PHCTEX, PHCTEY	°	Constant added to the phase distribution in X and Y polarizations.
RASHAPE	-	Shape of the reflectarray mask.

Table A1: Reflectarray parameters introduced in MRADANT-UPM.

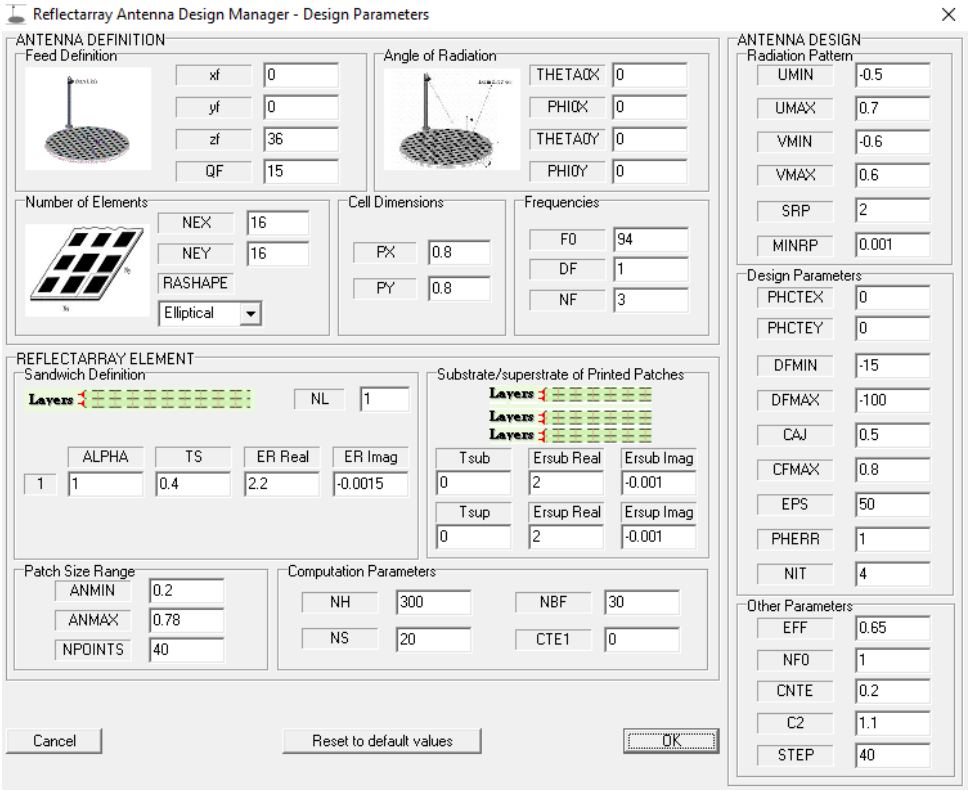

Figure A1: Preliminary design window of MRADANT-UPM.